## REFERENCES


Ahmed, S. R. Nano-Structure Materials. University of Maryland [Online]. 1999. Available from: http://www.glue.umd.edu/~srahmed/nanocomposite.html [2002, October 28].

Ahuja, S., and Kutty, T.R.N. Nanoparticles of $SrTiO_3$ prepared by gel to crystallite conversion.and their photocatalytic activity in the mineralization of phenol J. Photochem.Photobiol., A: Chem. 97 (1996): 99-107.

Alherici, R.M., and Jardim, W.F. Photocatalytic destruction of VOCs in the gas phase using titanium dioxide. Appl. Catal. B. 14 (1997): 55-68.

Ali, S., Chen, B., and Goodwin, Jr., J.G. Zr promotion of $Co/SiO_2$ for Fisher-Tropsch Synthesis. J. Catal. 157 (1995): 35-41.

Batista S. Marcelo, Elisabete M. Assaf, José M. Assaf and Edson A. Ticianelli. Double bed reactor for the simultaneous steam reforming of ethanol and water gas shift reactions. International Journal of Hydrogen Energy, 31 (2006): 1204.

Bibby D. M., and Dale, M. P. Synthesis of Silica-Sodalite form Non-aqueous Synthesis. Nature (London). 317 (1985): 157 – 158.

Bradley, D. C., Mehrotra, R. C., and Gaur, D. P. Metal Alkoxides. London, U.K., Academic Press, 1978.

Brik, Y., Kacimi, M., Ziyad, M., and Bozon-Verduraz, F. Titania-supported cobalt and cobalt-phosphorus catalysts: Characterization and performances in ethane oxidative dehydrogenation. J. Catal. 202 (2001): 118-128.

Campbell, L.K., Na, B.K., and Ko, E.I. Synthesis and characterization of titania aerogels. Chem. Mater. 4 (1992): 1329.

Cano F. Morales, Gijzeman O.L.J., de Groot F.M.F. and Weckhuysen B.M.. Manganese promotion in cobalt-based Fischer-Tropsch catalysis Studies in Surface Science and Catalysis, 147 (2004): 271.

Cheng, H., Ma, J., Zhao, Z., and Qi, L. Hydrothermal Preparation of Uniform Nanosize Rutile and Anatase Particle. Chem. Master. 7 (1995): 663 – 671.

Choi, J.G. Reduction of supporte cobalt catalysts by hydrogen. Catal Lett. 35 (1995): 291-296.

Coville, N.J., and Li, J. Effect of boron source on the catalyst reducibility and Fisher-Tropsch synthesis activity of o/$TiO_2$ catalysts. Catal. Today. 71 (2002): 403-410.

Cruickshack, M. C., and Glasser, L. S. D. A Penta-co-ordinated Aluminate Dimer; X-ray Crystal Structure. J. Chem. Soc., Chem. Commun. (1985): 84 – 85.

Dagan, G. and Tomkiewicz, M. Preparation and Characterization of $TiO_2$ Aerogel for Use as Photocatalysis. J. Non-Cryst. Solids. 175, 2-3 (1994):294 – 302.

Dalai, A.K., Das, T.K., Chaudhari, K.V., Jacobs, G., and Davis, B.H. Fischer–Tropsch synthesis: Water effects on Co supported on narrow and wide-pore silica. Appl. Catal. A: General. 289 (2005): 135-142.

Duvenhage, D.J., and Coville, N.J. Fe:Co/$TiO_2$ bimellic catalysts for the Fischer-Tropsch reaction Part 2. The effect of calcination and reduction temperature. Appl. Catal. A. 233(2002): 63-75.

Farrauto, R.J. and Bartholomew, C.H. Fundamentals of industrial catalytic processes. 1 st ed. London: Chapman & Hall, 1997.

Feller, A., Claeys, M., and Steen, EV. Cobalt cluster effects in zirconium promoted Co/$SiO_2$ Fischer–Tropsch Catalysts. J. Catal. 185 (1995): 20-130.

Fotou, G.P., and Pratsinis, S.E. Photocatalytic destruction of phenol and salicylic acid with aerosol-made and commercial titania powders. Chem. Eng. Comm. 151 (1996): 251-269.

Fox, M. A. and Dulay, M. T. Heterogeneous Photocataysis. Chem. Rev. 93 (1993): 341 – 357.

Fujishima, A., and Honda, K. Electrochemical photolysis of water at a semiconductor electrode. Nature (London). 37 (1972): 238.

Fujishima, A., Hashimoto, K., and Watanabe, T., $TiO_2$ photocatalysis: fundamental and applications. 1 st ed. Tokyo:BKC, 1999.

Fujiwara, H., Hosokawa, H., Murakoshi, K., Wada, Y., Yanagida, S., Okada, T., and Kobayashi, H. Effect of Surface Structures on Photocatalytic $CO_2$ Reduction Using Quantized CdS Nanocrystallites. J. Phys. Chem. B. 101 (1997): 8270.

Gao, X., and Wachs, I.E. Titania-silica as catalysts: molecular structural characteristics and physico-chemical properties. Catal. Today. 51 (1999): 233-254.

George, A.O. and Arpad, M. Hydrocarbon chemistry. New York:John Wiley & Sons, Inc.,1995.

Herrmann, J-M., Tahiri, H., Ait-Icho, Y., Lassaletta, G., Gonzalez-Elipe, A. R., and Fernadez, A. Characterization and Photocataytic Activity in Aqueous Medium of $TiO_2$ and Ag-$TiO_2$ Coatings on Quartz. Appl. Catal. B. 13 (1997): 219 – 228.

Hirano, M., Nakahara, C., Ota, K., and Inagaki, M. Direct Formation of Zirconia-Doped Titania with Stable Anatase-Type Structure by Thermal Hydrolysis. J. Am. Ceram. Soc. 85, 5 (2002): 1333 – 1335.

Howe, R.F., and Gratzel, M. EPR EPR Observation of Trapped Electrons in Colloidal $TiO_2$ J. Phys. Chem. 89 (1985) 4495.

Howe, R.F., and Gratzel, M. EPR Study of Hydrated Anatase under UV Irradiation J. Phys. Chem. 91 (1987) 3906.

Hu, S., Willey, R.J., and Notari, B. An investigation on the catalytic properties of titania-silica materials. J. Catal. 220 (2003): 240-248.

Iglesis, E., Soled, S.L., Fiato, R.A., and Via, G.H. Dispersion, Support and bimetallic effects in Fischer-Tropsch synthesis on cobalt catalysts. Natural Gas Conversion II. 81 (1994):433-442.

Inomata, M., Miyamoto, A., and Murakami, Y. Promoting Effect of $TiO_2$ and $Al_2O$ Supports on the Activity of Vanadium Oxide Catalyst for the Oxidation of Benzene Measured in Terms of the Turnover Frequency. J. Chem. Soc., Chem. Commun. (1980): 223.

Inoue, M., Kominami, H., and Inui, T. Reaction of Aluminium Alkoxides with Various Glycols and the Layer Structure of Their product. J. Chem. Soc., Dalton Trans. (1991): 3331 – 3336.

Inoue, M., Otsu, H., Kominami, H., and Inui, T. Synthesis of Yttrium Aluminiate Garmet by the Glycothermal Method. J. Am. Ceram. Soc. 74 (1991): 1452 – 1454.

Inoue, M., Nishikawa, T., and Inui, T. Glycothermal Synthesis of Rare Earth Iron Garnets. J. Mater. Res. 13, 4 (1998): 856 – 859.

Ishitani, O., Inoue, T., Suzuki, K., and Ibusuki,,T. Photocatalytic reduction of carbon dioxide to methane and acetic acid by an aqueous suspension of metal-deposited $TiO_2$. J. Photochem.Photobiol., A: Chem. 72 (1993): 269.

Iwamoto, S., Saito, K., Inoue, M., and Kagawa, K. Preparation of the Xerogels of Nanocrystalline Titanias by the Removal of the Glycol at the Glycothermal Method and Their Enhanced Photocatalytic Actitvities. Nano. Lett. 1, 8 (2001): 417 – 421.

Jacob, K., William, J.A., Jr., and Ernest, G. Inorganic chemistry. Boston: D.C. Heath and company, 1960.

Jacobs, G., Das, T.K., Zhang, Y., Li, J., Racoillet, G., and Davis, B.H. Fischer-Tropsch synthesis: support, loading, and promoter effects on the reducibility of cobalt catalysts. Appl. Catal. A. 233 (2002): 263-281.

John, J.M. Chemical processing handbook. New York: Marcel Dekker,Inc., 1993.

Jongsomjit, B., Panpranot, J., and Goodwin, J.G., Jr. Co-support compound formation in alumina-supported cobalt catalysts. J. Catal. 204 (2001): 98-109.

Jongsomjit, B., and Goodwin, J.G., Jr. Co-support compound formation in $Co/Al_2O_3$ catalysts: effect of reduction gas containing CO. Catal. Today. 77 (2002): 191-204.

Jongsomjit, B., Panpranot, J., and Goodwin, J.G., Jr. Effect of zirconia-modified alumina on the properties of $Co/g\text{-}Al_2O_3$ catalysts. J. Catal. 215 (2003): 66-77.

Jongsomjit, B., Sakdamnuson, C., Goodwin, J.G., Jr., and Praserthdam, P. Co-support compound formation in titania-supported cobalt catalyst. Catal. Lett. 94 (2004): 209-215.

Jongsomjit, B., Sakdamnuson, C., and Praserthdam, P. Dependence of crystalline phases in titania on catalytic properties during CO hydrogenation of $Co/TiO_2$ catalysts. Mat. Chem. and Phys. 89 (2005): 395-401.

Jongsomjit B., Wongsalee T., and Praserthdam P., Characteristics and catalytic properties of $Co/TiO_2$ for various rutile:anatase ratios Catalysis Communications. 6 (2005): 705-710.

Jung, K.Y., and Park, S.B. Anatase-phase titania: preparation by embedding silica and photocatalytic activity for the decomposition of trichloroethylene. J. Photochem. Photobiol., A: Chem.127 (1999): 177-122.

Kaliszewski, M. S., and Heuer, A. H. Alcohol Interaction with Zirconia Powder. J. Am. Ceram. Soc. 73, 6 (1990): 1504 - 1509.

Kamat, P. V. and Dimitrijevic, N. M. Colliodal Semiconductors as Photocatalysts for Solar Energy Conversion. Sol. Energy. 44, 2 (1990): 83 – 98.

Keesmann, I. Hydrothermal Synthesis of Brookite. Z. Anorg. Allg. Chem. 346 (1966): 30 – 43.

Kin, S. J., Park, S. D., Jeong, Y. H., and Park, S. Homogenous Precipitation of $TiO_2$ Ultrafine Powders from Aqueous $TiOCl_2$ Solution. J. Am. Ceram. Soc. 82, 4 (1999): 927 – 932.

Kogelbauer, A., Weber, J.C., and Goodwin, J.G., Jr. The formation of cobalt silicates on $Co/SiO_2$ under hydrothermal conditions. Catal Lett. 34 (1995): 259-267.

Kominami, H., Kato, J., Takada, Y., Doushi, Y., and Ohtani, B. Novel Synthesis of Microcrystalline Titanium (IV) Oxide having High Thermal Stability and Ultra-High Photocatalytic Activity: Thermal Decomposition of Titanium (IV) Alkoxide. Catal. Lett. 46 (1997): 235 – 240.

Kominami, H., Kato, J., Murakami, S., Kera, Y., Inoue, M., Inui, T., and Ohtani, B. Synthesis of Titanium (IV) Oxide of Ultra-High Photocatalytic Activity: High Temperature Hydrolysis of Titanium Alkoxides with Water Liberated Homogeneously from Solvent Alcohols. J. Mol. Catal. A. 144 (1999): 165 – 171.

Kominami, H., Kohno, M., Takada, Y., Inoue, M., Inui, T. Kera, Hydrothermal of Titanium Alkoxide in Organic Solvent at High Temperatures: A New Synthetic Method for Nanosized, Thermally Stable Titanium (IV) Oxide. Ind. Eng. Chem. Res. 38 (1999): 3925-3931.

Kominami, H., Onoue, S.-I., Matsuo, K., and Kera, Y. Synthesis of Microcrystalline Hematite and Magnetite in Organic Solvents and Effect of a small Amount of Water in Solvents. J. Am. Ceram. Soc. 82 (1999): 1937 – 1940.

Kominami, H., Murakami, S.-y., Kohno, M., Kera, Y., Okada, K., and Ohtani, B. Stoichiometric decomposition of water by titanium(IV) oxide photocatalyst synthesized in organic media: Effect of synthesis and irradiation conditions on photocatalytic activity. Phys. Chem. 3 (2001): 4102.

Kominami, H., Inoue, H., Konishi, S., and Kera, Y. Synthesis of Perovskite-Type Lanthanum Iron Oxide by Glycothermal Reaction of A Lanthanum-Iron Precursor. J. Am. Ceram. Soc. 85, 9 (2002): 2148 – 2150.

Kraum M. and Baerns M., Fischer–Tropsch synthesis: the influence of various cobalt compounds applied in the preparation of supported cobalt catalysts on their performance. Applied Catalysis A: General, 186 (1999): 189-200.

Kraum, M., and Baerns, M. Fischer-Tropsch synthesis: the influence of various cobalt compounds applied in the preparation of supported cobalt catalysts on their performance. Appl. Catal. A. 186 (2002): 189-200.

Kudo, A., Domen, K., Maruya, K., and Onishi, T. Photocatalytic activities of $TiO_2$ loaded with NiO. Chem.Phys. Lett. 133 (1987): 517.

Larson, S. A. and Falconer, J. L. Characterization of $TiO_2$ Photocatalysts Used in Trichloroethene Oxidation. Appl. Catal. B: Env. 4 (1994): 325 – 342.

Lee, Y. C., Hong, Y. P., Lee, H. Y., Kim, H., Jung, Y. J., Ko, K. H., Jung, H. S., and Kong, K. S. Photocatalysis and Hydrophilicity of Doped $TiO_2$ Thin Films.J. Colloid Interface Sci. 267 (2003): 127–131.

Li, J., and Coville, N.J.The effect of boron on the catalyst reducibility and activity of $Co/TiO_2$ Fischer-Tropsch catalysts. Appl. Catal. A. 181(1999): 201-208.

Li, J., and Coville, N.J. Effect of boron on the sulfur poisoning of $Co/TiO_2$ Fischer-Tropsch catalysts. Appl. Catal. A. 208 (2002): 177-184.

Li, J., and Coville, N.J. Effect of boron source on the catalyst reducibility and Fischer-Tropsch synthesis activity of $Co/TiO_2$ catalysts. Catal. Today. 71 (2002): 403-410.

Li, J., Jacobs, G., Zhang, Y., Das, T., and Davis, B.H. Fisher-Tropsch synthesis: effect of small amounts of boron, ruthenium and rhenium on $Co/TiO_2$ catalysts. Appl. Catal. A: General. 223 (2002): 195-203.

Li, J., Jacobs, G., Zhang, Y., Das, T., and Davis, B.H. Fisher-Tropsch synthesis: effect of water on the catalytic properties of a ruthenium promoted $Co/TiO_2$ catalysts. Appl. Catal. A: General. 233 (2002): 255-262.

Li, J.L., Xu, L.G., Keogh, R., and Davis, B. Fischer-Tropsch synthesis. Effect of CO pretreatment on a ruthenium promoted $Co/TiO_2$. Catal Lett. 70 (2000): 127-130.

Litter, M.L. Heterogeneous photocatalysis transition metal ions in photocatalytic systems. Appl. Catal. B:Environmental 23 (1999): 89-114.

Loddo, V., Marci, G., Martin, C., Palmisano, L., Rives, V., and Sclafani, A. Preparation and characterisation of $TiO_2$ (anatase) supported on $TiO_2$ (rutile) catalysts employed for 4-nitrophenol photodegradation in aqueous medium and comparison with $TiO_2$ (anatase) supported on $Al_2O_3$. Appl. Catal. B. 20 (1999): 29.

Luck, F. A Reviewer of Support Effect on the Activity and Selectivity of Hydrotreating Catalysts. Bull. Soc. Chim. Belg. 100 (1991): 781.

Madikizela, N.N., and Coville, N.J. A study of $Co/Zn/TiO_2$ catalysts in the fischer-Tropsch reaction. J. Mol. Catal. A. 181 (2002): 129-136.

Matsuda, S., and Kato, A. Titanium Oxide Based Catalysts-a Review. Appl. Catal. 8 (1983): 149.

McGraw-Hill encyclopedia of science & technology, New York, McGraw-Hill Book, 5 th ed., 1982: 435.

Montoya, I. A., Viveros, T., Domínguez, J.M., Canales, L.A., and Schifer, I. On the Effect of the Sol-Gel Synthesis Parameters on Textural and Structural Characteristics of $TiO_2$. Catal. Lett. 15 (1992): 207 – 217.

Moon, Y. T., Park, H. K., Kim, D. K., Kim, C. H., and Seog, I-S. Precipitation of Monodisperse and Spherical Zirconia Powders by Heating of Alcohol-Aqueous Salt Solution. J. Am. Ceram. Soc. 78, 10 (1995):2690 –2694.

Mohamed, M.M., Salama, T.M., and Yamaguchi, T. Synthesis, characterization and catalytic properties of titania–silica catalysts Colloids and Surfaces A: Physicochemical and Engineering Aspects. 207 (2002): 25-32.

Moradi, G.R., Basir, M.M., Taeb, A., and Kiennemann, A. Promotion of $Co/SiO_2$ Fischer–Tropsch catalysts with zirconium. Catal. Comm. 4 (2003): 27-32.

Nakaoka, Y., and Nosaka, Y. ESR Investigation into the effects of heat treatment and crystal structure on radicals produced over irradiated Ti02 powder J. Photochem. Photobiol., A: Chem. 110 (1997) 299.

Nagaoka, K., Takanabe, K., and Aika, K. Influence of the reduction temperature on catalytic activity of $Co/TiO_2$ (anatase-type) for high pressure dry reforming of methane. Appl. Catal. A. 255 (2003): 13-21.

Nagaoka, K., Takanabe, K., and Aika, K. Modification of $Co/TiO_2$ for dry reforming of methane at 2 MPa by Pt, Ru or Ni. Appl. Catal. A: General. 268 (2004): 151-158.

Nishimoto, S.-i., Ohtani, B., Yoshikawa, T., and Kagiya, T. Photocatalytic conversion of primary amines to secondary amines and cyclization of polymethylene-.alpha.,.omega.-diamines by an aqueous suspension of titanium(IV) oxide/platinum. J. Am.Chem. Soc. 105 (1983): 7180.

Nobuntu, N., Madikizela, M., and Coville, N.J. Surface and reactor study of the effect of zinc on titania-supported Fischer-Tropsch cobalt catalysts. Appl. Catal. A: General 272 (2004): 339-346.

Ollis, D.F. Heterogeneous photocatalysis. CATECH. 2 (2) (1998): 149-157.

Ogihara, T., Nakajima, H., Yanagawa, T., Ogata, N., Yoshida, K., and Matsushita, N. Preparation of Monodisperse, Spherical Alumina Powders from Alkoxides. J. Am. Ceram. Soc. 74, 9 (1991): 2263 – 2269.

Ohtani, B., Ogawa, Y., and Nishimoto, S.-i. Photocatalytic Activity of Amorphous-Anatase Mixture of Titanium(IV) Oxide Particles Suspended in Aqueous Solutions. J. Phys. Chem. B. 101 (1997): 3746-3752.

Othmer, K. Encyclopedia of chemical technology. Vol. 6. 4 th ed. New York: A Wiley-Interscience Publication, John Wiley&Son, 1991.

Panpranot, J., Goodwin, J.G., Jr., and Sayari, A. CO hydrogenation on Ru-promoted Co/MCM-41 catalysts. J. Catal. 211 (2002): 530-539.

Park, D.R., Zhang, J., Ikeue, K., Yamashita, H., and Anpo, M. Photocatalytic Oxidation of Ethylene to $CO_2$ and $H_2O$ on Ultrafine Powdered $TiO_2$ Photocatalysts in the Presence of $O_2$ and $H_2O$. J. Catal. 185 (1999): 114–119.

Park, H.K., Kim, D.K., and Kim, C.H. Effect of Solvent on Titania Particle Formation and Morphology in Thermal Hydrolysis of $TiCl_4$. J. Am. Ceram. Soc. 80, 3 (1997): 743 – 749.

Payakgul, W., Mekasuwandumrong O., Pavarajarn V., and Praserthdam P. Effects of reaction medium on the synthesis of TiO2 nanocrystals by thermal decomposition of titanium (IV) n-butoxide. Ceram Inter. 31 (2005): 391–397

Popielaski, S. Photocatalysis on Nano-Sized Semiconductors. Rensselaer[Online]. 1998. Available from: http://www.rpi.edu/locker/25/001225/public_html/New%20Folder/ popielarski/[2002, October 28]

Readey, M. J., Lee, R., Holloran, J. W., and Heuer, A. H. Processing and Sintering of Ultrafine MgO-$ZrO_2$ and ($MgO,Y_2O_3$)$ZrO_2$ Powder. J. Am. Ceram. Soc. 73, 6 (1990): 1499 - 1503.

Pradyot Patnaik, Ph.D. Handkook of inorganic chemicals. New York: McGraw-Hill, 2002.

Price, J.G., Glasser, D., Hildebrandt, D., and Coville, N.J. Fischer-Tropsch synthesis: DRIFTS and SIMS surface investigation of Co and Co/Ru on titania supports. Natural Gas Conversion IV. 107 (1997): 243-248.

Rana, M.S., Maity, S.K., Ancheyta, J., Murali Dhar, G., and Prasada Raob, T.S.R. $TiO_2$–$SiO_2$ supported hydrotreating catalysts: physico-chemical characterization and activities. Appl. Catal. A: General. 253 (2003): 165-176.

Reuel, R.C., and Bartholomew, C.H. The stoichiometries of $H_2$ and CO adsorption on cobalt: effects of support and preparation. J. Catal. 85 (1984): 63-77.

Riva, R., Miessner, H., and Piero, G.D. Metal-support interaction in $Co/SiO_2$ and $Co/TiO_2$. Appl. Catal. A. 196 (2000): 111-123.

Rohr, F., Lindvåga, O.A., Holmenb, A., and Blekkanb, E.A. Fischer–Tropsch synthesis over cobalt catalysts supported on zirconia-modified alumina. Catal. Today. 58 (2000): 247-254.

Sato, S., and White, J. M. Photodecomposition of water over $Pt/TiO_2$ catalysts. Chem. Phys. Lett. 72 (1980): 83.

Schiavello, M. Heterogeneous Photocatalysis. Ed.; John Wiley &Sons: New York, 1997.

Schanke, D., Hilmen, A.M., Bergene, E., Kinnari, K., Rytter, E.,Adnanes, E., and Holmen, A. Study of the deactivation mechanism of $Al_2O_3$-supported cobalt Fischer-Tropsch catalysts. Catal Lett. 34 (1995): 269-284.

Sepone, N., and Pelizzetti, E. Photocatalysis: Fundamentals and Applications. Eds.; John Wiley & Sons: New York, 1989.

Shinoda, M., Zhang, Y., Yoneyama, Y., Hasegawa, K., and Tsubaki, N. New bimodal pore catalysts for Fischer–Tropsch synthesis. Fuel Processing Tech. 86 (2004): 73-85.

Sornnarong Theinkeaw. Synthesis of Large-Surface Area Silica Modified Titanium (IV) Oxide Ultra Fine Particles. Master's thesis, Department of Chemical Engineering, Graduated School, Chulalongkorn University, 2000.

Storsæter, S., Borg, Ø., Blekkan, E.A., and Holmen, A. Study of the effect of water on Fischer–Tropsch synthesis over supported cobalt catalysts. J. Catal. 231 (2005): 405-419.

Sun, S., Fujimoto, K., Yoneyama, Y., and Tsubaki, N. Fisher-Tropsch synthesis using $Co/SiO_2$ catalysts prepared from mixed precursors and addition effect of noble metals. Fuel. 81 (2002): 1583-1591.

Tabata, S., Nishida, H., Masaki, Y., and Tabata, K. Stoichiometric photocatalytic decomposition of pure water in $Pt/TiO_2$ aqueous suspension system. Catal. Lett. 34 (1995): 245.

Takeda, S., Suzuki, S., Odaka, H., and Hosono, H. Photocatalytic $TiO_2$ Thin Film Deposited onto Glass by DC Magnetron Sputtering. Thin Solid Films. 392 (2001): 338-344.

Theinkaew, S., Synthesis of large-surface area silica midified titanium (IV) oxide ultrafine particles, Master's thesis, Faculty of Engineering, Chulalongkorn University, (2002).

Torimoto, T., Fox III, R.J., and Fox, M.A. Photoelectrochemical Doping of $TiO_2$ Particles and the Effect of Charge Carrier Density on the Photocatalytic activity of Microporous Semiconductor Electrode Films. J. Electrochem. Soc. 143(11) (1996): 3712-3717.

Tsubaki, N., Sun, S., and Fujimoto, K. Different function of the noble metals added to cobalt catalysts for Fischer-Tropsch synthesis. J. Catal. 199 (2001): 236-246.

Vob, M., Borgmann, D., and Wedler, G. Characterization of alumina, silica, and titania supported cobalt catalysts. J. Catal. 212 (2002): 10-21.

Wachiraphan Payakgul. Crystallization and Precipitation Mechanism of Titanium (IV) Oxide under The Solvothermal Condition and The Effect of Second Element on Titanium (IV) Oxide Products. Master's thesis, Department of Chemical Engineering, Graduated School, Chulalongkorn University, 2002.

Wang, C.C., Zhang, Z., and Ying, J.Y. Photocatalytic Decomposition of Halogenated Organics over Nanocrystalline. Titania Nanostr. Mater. 9 (1997) 583-586.

West, A. R.; Solid State Chemistry and its Application. Brisbane: John Wiley&Sons, 1997.

Xiong, H., Zhang, Y., Liew, K., and Li, J. Catalytic performance of zirconium-modified $Co/Al_2O_3$ for Fischer–Tropsch synthesis. J. Molecular Catal., A: Chemical 231 (2005): 145-151.

Yang, J., Mei, S., and Ferreira, M. F. Hydrothermal Synthesis of Nanosized Titania Powders: Influence of Tetraalkyl Ammonium Hydroxides on particle Characteristic. J. Am. Ceram. Soc. 84, 8 (2001): 1696 – 1702.

Yanagisawa, K., Ioku, K., and Yamasaki, N. Formation of Anatase Porous by Hydrothermal Hot-Pressing of Amorphous Titania Spheres. J. Am. Ceram. Soc. 8, 5 (1997): 1303 – 1306.

Yin, S., Inoue, Y., Uchida, S., Fujisiro, Y., and Sato, T. Crystallization of titania in liquid media and photochemical properties of crystallized titania. J. Mater. Res. 13, 4 (1998): 844 -847.

Yogarasimhan, S. R. and Rao, C. N. Mechanism of Crystal Structure Transformations. Trans. Faraday Soc. 58 (1962): 1579 – 1589.

Yoshinaka, M., Hirota, K., and Yamaguchi, O. Formation and Sintering of $TiO_2$ (Anatase) Solid Solution in the System $TiO_2$-$SiO_2$. J. Am. Ceram. Soc. 80, 10 (1997): 2749 – 2753.

Young, R.S. COBALT: Its Chemistry, Metallurgy, and Uses. New York: Reinhpld Publishing Corporation, 1960.

Zaharescu, M., Crisan, M., Simionescu, L., Crisan, D., and Gartner, M. TiO2-Based Porous Materials obtained from Gels, in Different Experimental Conditions. J. Sol-Gel Sci. 8, 1-3 (1997): 249 – 253.

Zhang, H., Finnegan, M., and Banfield, J. F. Preparing Single-Phase Nanocrystalline Anatase from Amorphous Titania with Particle Size Tailed by Temperature. Nano. Lett. 1, 2 (2001): 81 – 85.

Zzanderna, A. W., Rao, C. N. R., and Honig, J. M. The Anatase-Rutile Transition. Trans. Faraday Soc. 58 (1958): 1069 – 1073.

Zennaro, R., Tagliabue, M., and Bartholomew, C.H. Kinetics of Fischer-Tropsch synthesis on titania-supported cobalt. Catal. Today. 58 (2000): 309-319.

Zhang, Y., Shinoda, M., and Tsubaki, N. Development of bimodal cobalt catalysts for Fischer–Tropsch synthesis. Catal. Today. 93-95 (2004): 55-63.

Zhang, Y., Wei, D., Hammache, S., and Goodwin, J.G., Jr. Effect of water vapor on the reduction of Ru-promoted Co/$Al_2O_3$. J. Catal. 188 (1999): 281-290.

# APPENDICES

# APPENDIX A

## CALCULATION OF THE CRYSTALLITE SIZE

### Calculation of the crystallite size by Debye-Scherrer equation

The crystallite size was calculated from the half-height width of the diffraction peak of XRD pattern using the Debye-Scherrer equation.

From Scherrer equation:

$$D = \frac{K\lambda}{\beta \cos \theta} \qquad (A.1)$$

where D = Crystallite size, Å

K = Crystallite-shape factor = 0.9

λ = X-ray wavelength, 1.5418 Å for CuKα

θ = Observed peak angle, degree

β = X-ray diffraction broadening, radian

The X-ray diffraction broadening (β) is the pure width of a powder diffraction free of all broadening due to the experimental equipment. Standard α-alumina is used to observe the instrumental broadening since its crystallite size is larger than 2000 Å. The X-ray diffraction broadening (β) can be obtained by using Warren's formula.

From Warren's formula:

$$\beta^2 = B_M^2 - B_S^2 \qquad (A.2)$$

$$\beta = \sqrt{B_M^2 - B_S^2}$$

Where $B_M$ = The measured peak width in radians at half peak height.

$B_S$ = The corresponding width of a standard material.

**Example:** Calculation of the crystallite size of titania

The half-height width of 101 diffraction peak = 0.93125°

= 0.01625 radian

The corresponding half-height width of peak of α-alumina = 0.004 radian

The pure width = $\sqrt{B_M^2 - B_S^2}$

= $\sqrt{0.01625^2 - 0.004^2}$

= 0.01577 radian

$\beta$ = 0.01577 radian

$2\theta$ = 25.56°

$\theta$ = 12.78°

$\lambda$ = 1.5418 Å

The crystallite size = $\frac{0.9x\,1.5418}{0.01577\ \cos 12.78}$ = 90.15 Å

= 9 nm

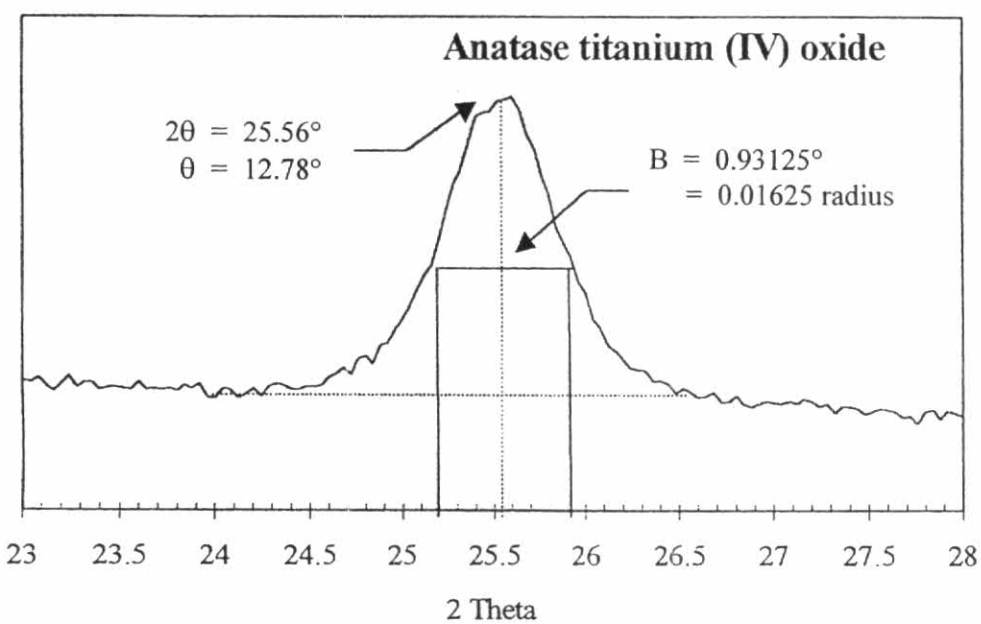


**Figure A.1** The 101 diffraction peak of titania for calculation of the crystallite size

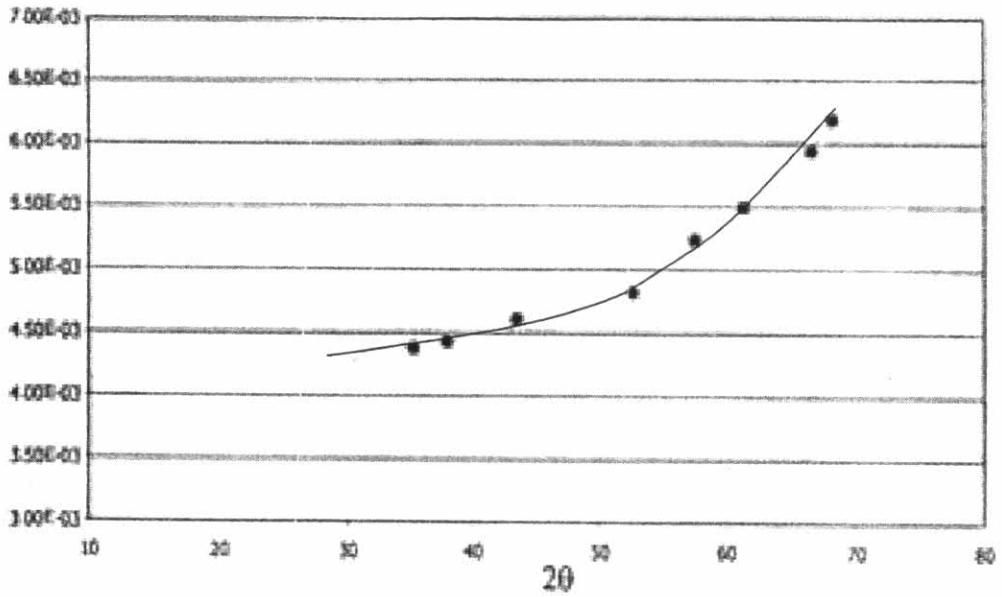


**Figure A.2** The plot indicating the value of line broadening due to the equipment. The data were obtained by using α-alumina as standard

# APPENDIX B

## CALCULATION FOR CATALYST PREPARATION

Preparation of $TiO_2$ support and 5, 10, 15 and 20 wt. % $Co/TiO_2$ catalysts by the incipient wetness impregnation method are shown as follows:

Reagent: - Titania (IV) buoxide ($TiO_2$)

Molecular weight = 131.5

- Cobalt (II) nitrate hexahydrate ($Co(NO_3)_2 \cdot 6H_2O$)

Molecular weight = 290.93

**Calculation for the preparation of cobalt loading catalyst (20 wt. % $Co/TiO_2$)**

Based on 100 g of catalyst used, the composition of the catalyst will be as follows:

Cobalt = 20 g

Titania = 100-20 = 80 g

For 5 g of titania

Cobalt required = $5 \times (20/80)$ = 1.25 g

Cobalt 1.25 g was prepared from $Co(NO_3)_2 \cdot 6H_2O$ and molecular weight of Co is 58.93

$$Co(NO_3)_2 \cdot 6H_2O \text{ required} = \frac{\text{MW of } Co(NO_3)_2 \cdot 6H_2O \times \text{cobalt required}}{\text{MW of Co}}$$

$$= (290.93/58.93) \times 1.25 = 6.17 \text{ g}$$

Dissolve of Cobalt (II) nitrate hexahydrate and volume of de-ionized water like preparation of unpromoted catalyst.

# APPENDIX C

## THE OPERATING CONDITIONS OF GAS CHROMATOGRAPHY

The composition of hydrocarbons in the product stream was analyzed by a Shimadzu GC14B gas chromatograph equipped with a flame ionization detector. The operating conditions for each instrument are shown in the Table C.1.

**Table C.1** The operating condition for gas chromatograph.

| Gas Chromagraph | SHIMADZU GC-14B |
|---|---|
| Detector | FID |
| Column | VZ10 |
| Carrier gas | $H_2$ (99.999%) |
| Carrier gas flow (ml/min) | 30 cc/min |
| Column temperature | |
| - initial ($^oC$) | 70 |
| - final ($^oC$) | 70 |
| Injector temperature ($^oC$) | 100 |
| Detector temperature ($^oC$) | 150 |
| Current (mA) | - |
| Analysed gas | Hydrocarbon $C_1$-$C_4$ |

The calibration curves for calculation of composition of reactant in photocatalytic reaction. The reactant is ethylene.

The VZ10 column are used with a gas chromatography equipped with a flame ionization detector, Shimadzu modal 14B, to analyze the concentration of products including of ethylene.

Mole of reagent in y-axis and area reported by gas chromatography in x-axis are exhibited in the curves. The calibration curve of ethylene is illustrated in the following figure.

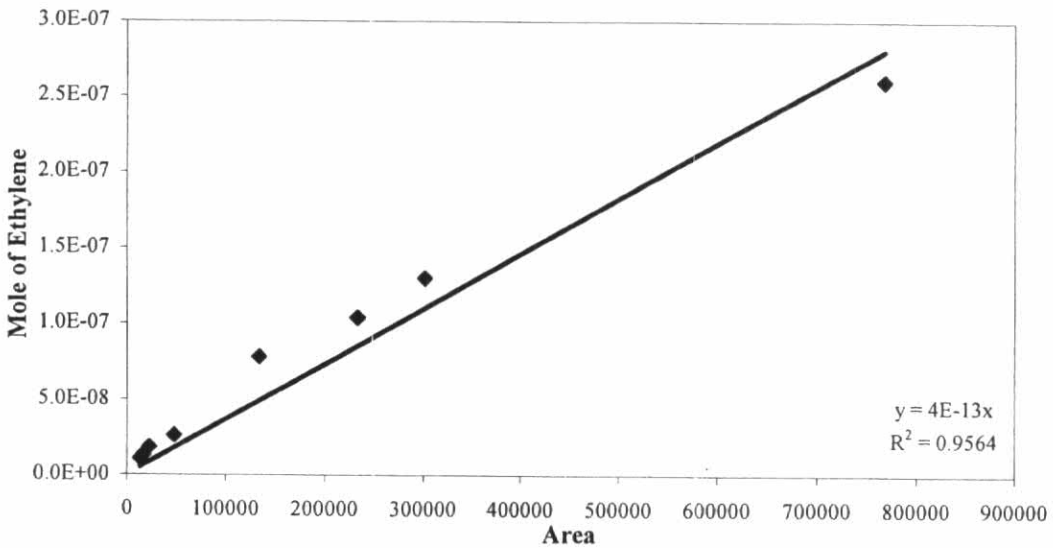


**Figure C.1** The calibration curve of ethylene.

# APPENDIX D

## CALCULATION FOR REDUCIBILITY

For supported cobalt catalyst, it can be assumed that the major species of calcined Co catalysts is $Co_3O_4$. $H_2$ consumption of $Co_3O_4$ is calculated as follows:

Molecular weight of Co = 58.93

Molecular weight of $Co_3O_4$ = 240.79

**Calculation of the calibration of $H_2$ consumption using cobalt oxide ($Co_3O_4$)**

Let the weight of $Co_3O_4$ used = 0.01 g

= $4.153\times10^{-5}$ mole

From equation of $Co_3O_4$ reduction;

$$Co_3O_4 + 4H_2 \rightarrow 3Co + 4H_2O \qquad (D.1)$$

$H_2$ = 4 $Co_3O_4$

= $4\times4.153\times10^{-5}$ = $1.661\times10^{-4}$ mole

Integral area of $Co_3O_4$ after reduction = 396572.5 unit

Thus, the amount of $H_2$ that can be consumed at 100 % reducibility is $1.661\times10^{-4}$ mole which related to the integral area of $Co_3O_4$ after reduction 396572.5 unit.

**Calculation of reducibility of supported cobalt catalyst**

| | | | |
|---|---|---|---|
| Integral area of the calcined catalyst | = | X | unit |
| The amount of $H_2$ consumption | = | $[1.661\times10^{-4}\times(X)/396572.5]$ | mole |
| Let the weight of calcined catalyst used | = | W | g |
| Concentration of Co | = | Y | % wt |
| Mole of Co | = | [(W×Y)/58.93] | mole |
| Mole of $Co_3O_4$ | = | [(W×Y)/3×58.93] | mole |

Mole of $H_2$ can be consumed = $[(W \times Y) \times 4/3 \times 58.93]$ mole

Reducibility (%) of supported Co catalyst = $\dfrac{[1.661 \times 10^{-4} \times (X)/396572.5] \times 100}{[(W \times Y) \times 4/3 \times 58.93]}$

# APPENDIX E

## CALCULATION FOR TOTAL $H_2$ CHEMISORPTION AND DISPERSION

Calculation of the total $H_2$ chemisorptions and metal dispersion of the catalyst, a stoichiometry of H/Co = 1, measured by $H_2$ chemisorptions is as follows:

| | | | |
|---|---|---|---|
| Let the weight of catalyst used | = | W | g |
| Integral area of $H_2$ peak after adsorption | = | A | unit |
| Integral area of 45 µl of standard $H_2$ peak | = | B | unit |
| Amounts of $H_2$ adsorbed on catalyst | = | B-A | unit |
| Concentration of Co | = | C | % wt |
| Volume of $H_2$ adsorbed on catalyst | = | 45×[(B-A)/B] | µl |
| Volume of 1 mole of $H_2$ at 100°C | = | 28.038 | µl |
| Mole of $H_2$ adsorbed on catalyst | = | [(B-A)/B]×[45/28.038] | µmole |

Total hydrogen chemisorptions = [(B-A)/B]×[45/28.038]×[1/W] µmole /g of catalyst

= N µmole /g of catalyst

Molecular weight of cobalt = 58.93

Metal dispersion (%) = $\dfrac{2\times H_{2\ tot}/\text{g of catalyst}\times 100}{\text{No µmole } Co_{tot}/\text{g of catalyst}}$

= $\dfrac{2\times N\times 100}{\text{No µmole } Co_{tot}}$

= $\dfrac{2\times N\times 58.93\times 100}{C\times 10^6}$

= $\dfrac{1.179\times N}{C}$

# APPENDIX F

## CALIBRATION CURVES

This appendix showed the calibration curves for calculation of composition of reactant and products in CO hydrogenation reaction. The reactant is CO and the main product is methane. The other products are linear hydrocarbons of heavier molecular weight that are $C_2$-$C_4$ such as ethane, ethylene, propane, propylene and butane.

The thermal conductivity detector, gas chromatography Shimadzu model 8A was used to analyze the concentration of CO by using Molecular sieve 5A column. The chromatograms of catalyst sample are shown in Figure F.1.

The VZ10 column are used with a gas chromatography equipped with a flame ionization detector, Shimadzu modal 14B, to analyze the concentration of products including of methane, ethane, ethylene, propane, propylene and butane. The chromatograms of catalyst sample are shown in Figure F.2. Conditions uses in both GC are illustrated in Table F.1.

Mole of reagent in y-axis and area reported by gas chromatography in x-axis are exhibited in the curves. The calibration curves of CO, methane, ethane, ethylene, propane, propylene and butane are illustrated in the following figures.

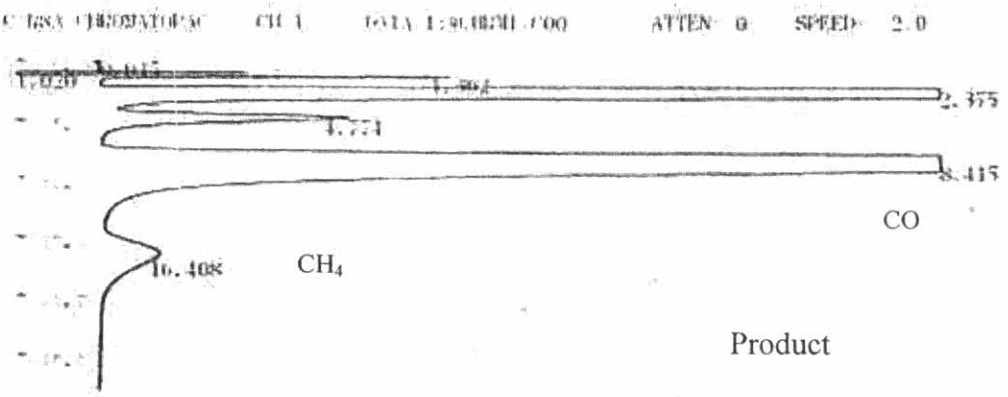


C-R8A CHROMATOPAC CH-1 Report No. 1 DATA=I:¥CHRM1.C00 01/09/06 10:31:56

** CALCULATION REPORT **

| CH | PKNO | TIME | AREA | HEIGHT | MK | UNO | CONC | NAME |
|---|---|---|---|---|---|---|---|---|
| 1 | 1 | 0.015 | 13 | 5 | | | 0.001 | |
| | 2 | 1.02 | 3410 | 1949 | | | 0.4017 | |
| | 3 | 1.302 | 76503 | 3630 | | | 5.7551 | |
| | 4 | 2.375 | 1011949 | 10254 | | | 76.1259 | |
| | 5 | 4.771 | 14440 | 295 | | | 1.0863 | |
| | 6 | 8.415 | 208953 | 2183 | | | 15.7189 | |
| | 7 | 16.408 | 12112 | 70 | | | 0.9111 | |
| | | TOTAL | 1329310 | 34685 | | | 100 | |

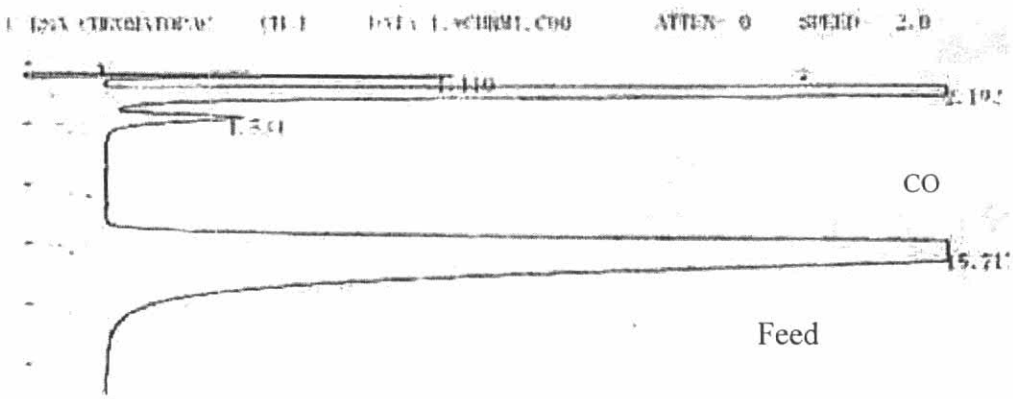


C-R8A CHROMATOPAC CH-1 Report No. 5 DATA=I:¥CHRM1.C00 01/09/06 12:44:10

** CALCULATION REPORT **

| CH | PKNO | TIME | AREA | HEIGHT | MK | UNO | CONC | NAME |
|---|---|---|---|---|---|---|---|---|
| 1 | 1 | 1.11 | 91504 | 4090 | | | 7.756 | |
| | 2 | 2.192 | 842590 | 38821 | | | 71.419 | |
| | 3 | 3.531 | 7861 | 163 | V | | 0.6663 | |
| | 4 | 15.717 | 237829 | 1428 | | | 20.1587 | |
| | | TOTAL | 1179781 | 44509 | | | 100 | |

**Figure F.1** The chromatograms of catalyst sample from thermal conductivity detector, gas chromatography Shimadzu model 8A (Molecular sieve 5A column).

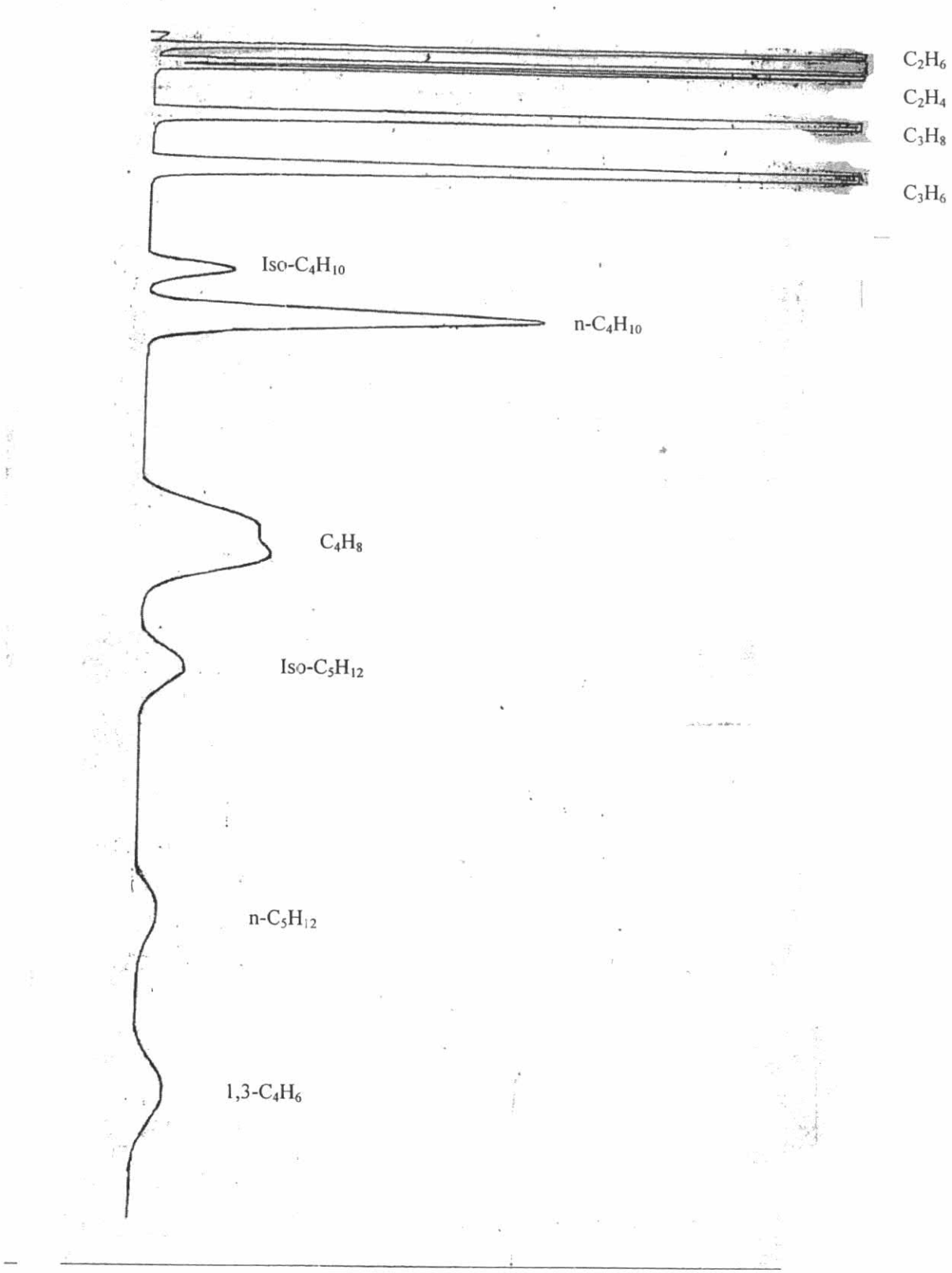


**Figure F.2** The chromatograms of catalyst sample from flame ionization detector, gas chromatography Shimadzu modal 14B (VZ10 column).

**Table F.1** Conditions use in Shimadzu modal GC-8A and GC-14B.

| Parameters | Condition | |
|---|---|---|
| | Shimadzu GC-8A | Shimadzu GC-14B |
| Width | 5 | 5 |
| Slope | 50 | 50 |
| Drift | 0 | 0 |
| Min. area | 10 | 10 |
| T.DBL | 0 | 0 |
| Stop time | 50 | 60 |
| Atten | 0 | 0 |
| Speed | 2 | 2 |
| Method | 41 | 41 |
| Format | 1 | 1 |
| SPL.WT | 100 | 100 |
| IS.WT | 1 | 1 |

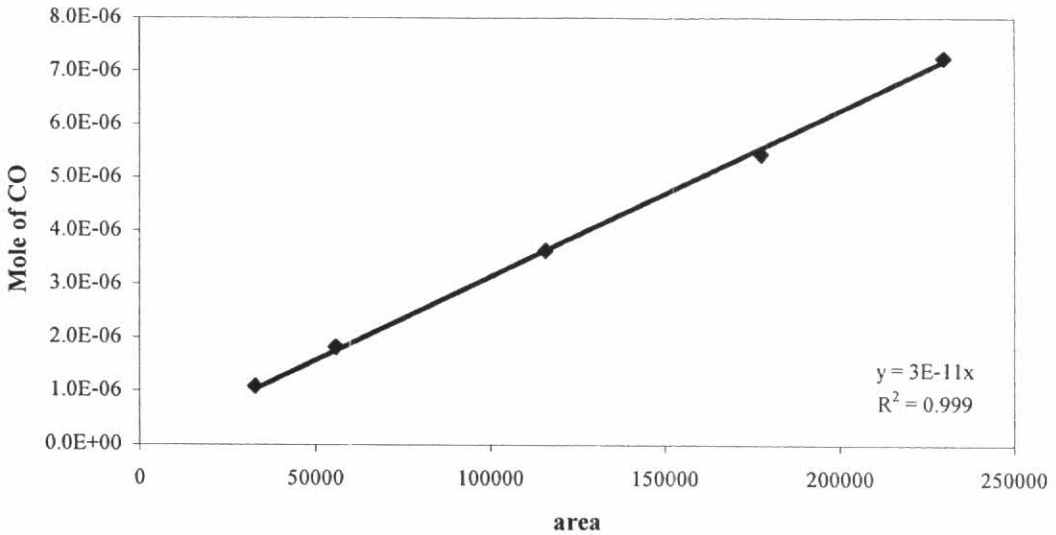


**Figure F.3** The calibration curve of CO.

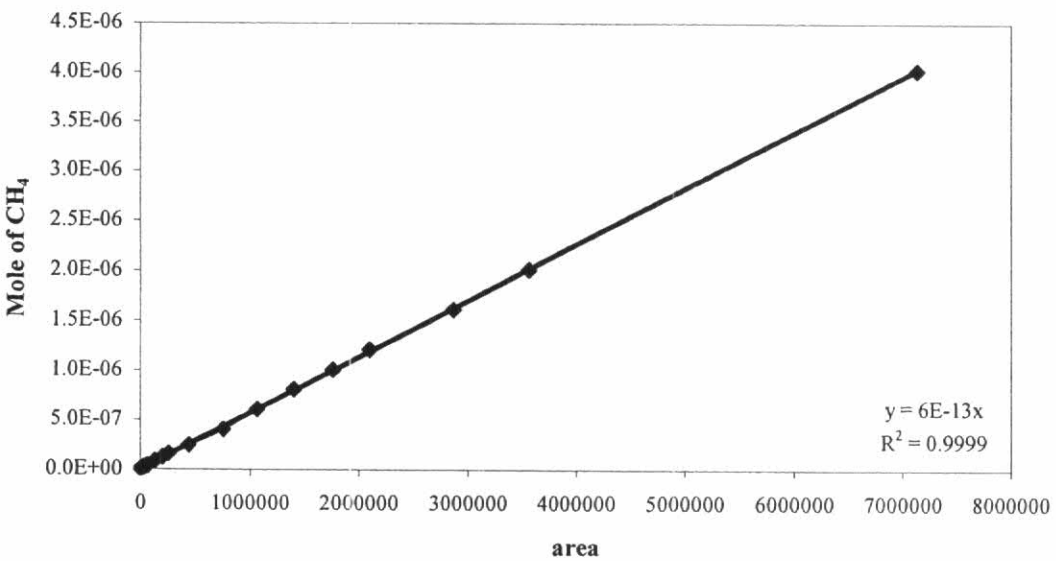


**Figure F.4** The calibration curve of methane.

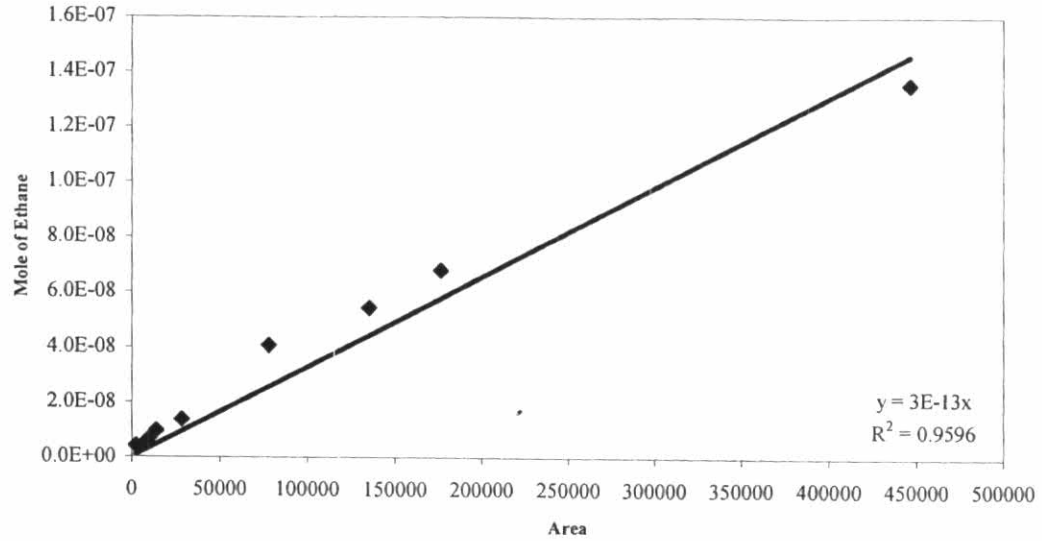


**Figure F.5** The calibration curve of ethane.

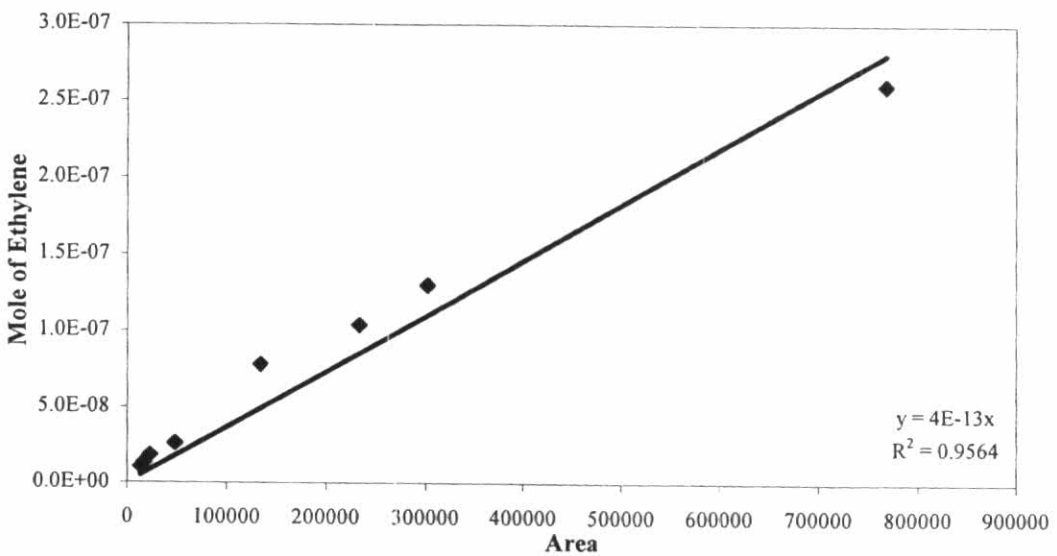


**Figure F.6** The calibration curve of ethylene.

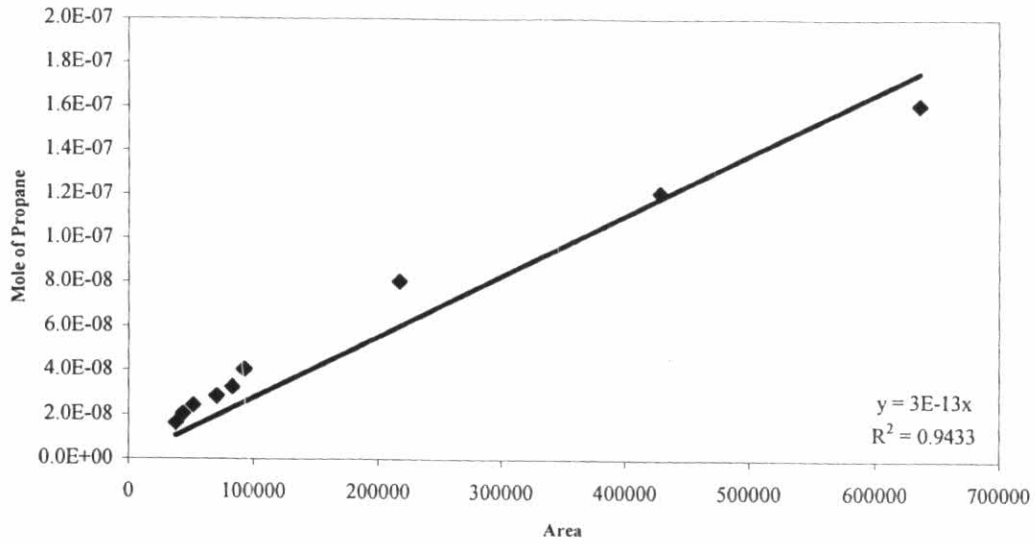


**Figure F.7** The calibration curve of propane.

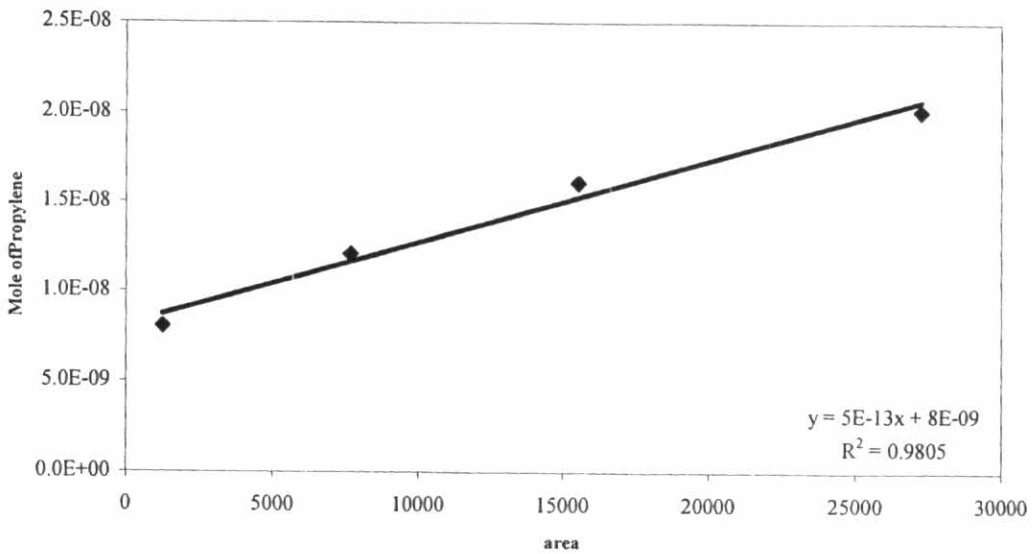


**Figure F.8** The Calibration curve of propylene.

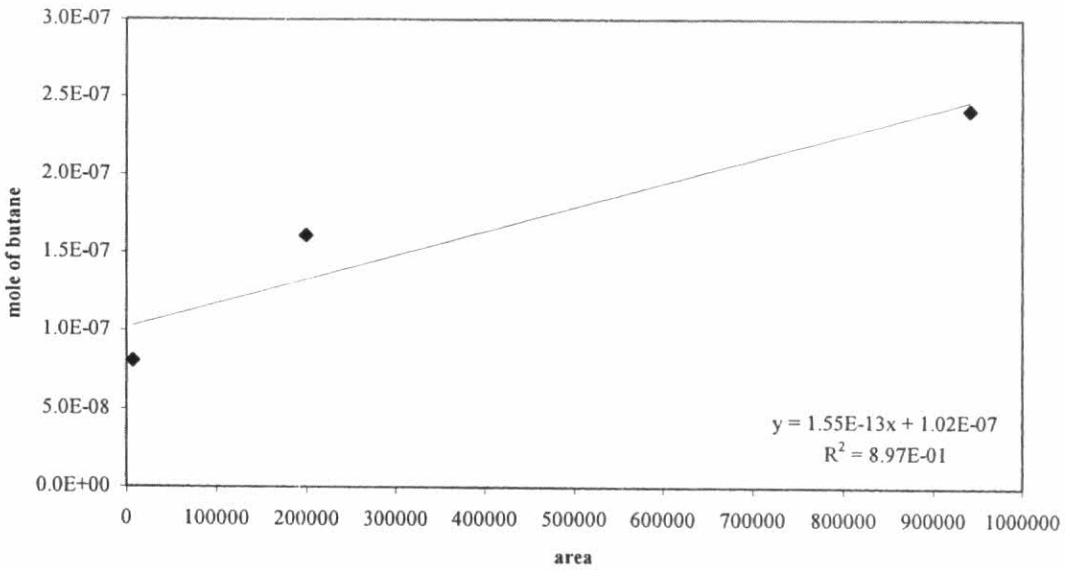


**Figure F.9** The calibration curve of butane

# APPENDIX G

## CALCULATION OF CO CONVERSION, REACTION RATE AND SELECTIVITY

The catalyst performance for the CO hydrogenation was evaluated in terms of activity for CO conversion reaction rate and selectivity.

Activity of the catalyst performed in term of carbon monoxide conversion and reaction rate. Carbon monoxide conversion is defined as moles of CO converted with respect to CO in feed:

$$\text{CO conversion (\%)} = \frac{100 \times [\text{mole of CO in feed} - \text{mole of CO in product}]}{\text{mole of CO in feed}} \quad \text{(i)}$$

where mole of CO can be measured employing the calibration curve of CO in Figure F.1, Appendix F.,i.e.,

$$\text{mole of CO} = (\text{area of CO peak from integrator plot on GC-8A}) \times 3 \times 10^{-11} \quad \text{(ii)}$$

Reaction rate was calculated from CO conversion that is as follows:

| | | | |
|---|---|---|---|
| Let the weight of catalyst used | = | W | g |
| Flow rate of CO | = | 2 | cc/min |
| Reaction time | = | 60 | min |
| Weight of $CH_2$ | = | 14 | g |
| Volume of 1 mole of gas at 1 atm | = | 22400 | cc |

$$\text{Reaction rate (g } CH_2\text{/g of catalyst/h)} = \frac{[\text{\% conversion of CO}/100] \times 60 \times 14 \times 2}{W \times 22400} \quad \text{(iii)}$$

Selectivity of product is defined as mole of product (B) formed with respect to mole of CO converted:

$$\text{Selectivity of B (\%)} = 100 \times [\text{mole of B formed/mole of total products}] \quad \text{(iv)}$$

Where B is product, mole of B can be measured employing the calibration curve of products such as methane, ethane, ethylene, propane, propylene and butane in Figure F.4-F.9, Appendix F.,i.e.,

mole of $CH_4$ = ( area of $CH_4$ peak from integrator plot on GC-14B)$\times 6\times10^{-13}$ (ii)

# APPENDIX H

## LIST OF PUBICATIONS

1. Wilasinee Kongsuebchart, Piyasan Praserthdam*, Joongjai Panpranot, Akawat Sirisuk, Piyawat Supphasrirongjaroen, and Chairit Satayaprasert, "Effect of Crystallite Size on the Surface Defect of Nano-$TiO_2$ Prepared via Solvothermal Synthesis", *Journal of Crystal Growth*, 297 (2006): 234-238.

2. Wilasinee Kongsuebchart, Joongjai Panpranot, Chairit Satayaprasert, and Piyasan Praserthdam, "Effect of $TiO_2$ Crystallite size on the Dispersion of Co on Nanocrystalline $TiO_2$", *Reaction Kinetics and Catalysis Letters*, 91 (2007): 119-126.

3. Wilasinee Kongsuebchart, Joongjai Panpranot, Chairit Satayaprasert, and Piyasan Praserthdam, "Effects of $TiO_2$ Crystallite Size and Co Loading on the Catalytic Properties of Nanocrystalline $TiO_2$-Supported Co Catalysts in CO Hydrogenation Reaction", *Catalysis Communications*, (in press).

Available online at www.sciencedirect.com
ScienceDirect
Journal of Crystal Growth 297 (2006) 234–238
JOURNAL OF CRYSTAL GROWTH
www.elsevier.com/locate/jcrysgro

# Effect of crystallite size on the surface defect of nano-$TiO_2$ prepared via solvothermal synthesis

Wilasinee Kongsuebchart, Piyasan Praserthdam*, Joongjai Panpranot, Akawat Sirisuk, Piyawat Supphasrirongjaroen, Chairit Satayaprasert

*Center of Excellence on Catalysis and Catalytic Reaction Engineering, Department of Chemical Engineering, Faculty of Engineering, Chulalongkorn University, Bangkok 10330, Thailand*

Received 21 June 2006; received in revised form 31 August 2006; accepted 2 September 2006
Communicated by J. M. Redwing
Available online 20 November 2006

**Abstract**

Nano-$TiO_2$ powders were synthesized by the solvothermal method under various reaction conditions in order to obtain average crystallite sizes of 9–15 nm. The amounts of surface defect of $TiO_2$ were measured by means of temperature-programmed desorption of $CO_2$ and electron spin resonance spectroscopy. It was found that the ratios of surface defect/specific surface area increased significantly with increasing $TiO_2$ crystallite size. The $TiO_2$ with higher amounts of surface defects exhibited much higher photocatalytic activity for ethylene decomposition.


*Keywords:* A1. Crystallite size; A1. Surface defect; A1. Surface structure; B1. $TiO_2$; B1. $Ti^{3+}$

## 1. Introduction

Nowadays, titanium (IV) dioxide or titania ($TiO_2$) is one of the most popular and promising catalysts in photocatalytic applications for environmental remediation due to the strong oxidizing power of its holes, high photostability, and redox selectivity [1–7]. Titania can be synthesized by various methods such as solvothermal method [8–11], precipitation method [12], sol–gel method [13–15], and thermal decomposition of alkoxide [16]. The properties of $TiO_2$ synthesized by different methods vary in terms of their crystal structure, chemical composition, surface morphology, crystal defects, specific surface area, etc. While the sol–gel method is widely used to prepare nano-sized $TiO_2$, the precipitated powders obtained are amorphous in nature and further heat treatment is required for crystallization. The solvothermal method is an alternative route for one-step synthesis of pure anatase nano-sized $TiO_2$. Particle morphology, crystalline phase, and surface chemistry of the solvothermal-derived $TiO_2$ can be easily controlled by regulating precursor composition, reaction temperature, pressure, solvent property, and aging time [17].

There always exist structural defects on the surface and inside titania particles [18]. These structural defects are related with the density of photoexcited electrons. Surface defects are good for high photocatalytic activity because they can act as active sites for adsorption and dissociation of molecules on the $TiO_2$ surface [19–21]. However, the bulk defect lowers the photocatalytic activity because they provide sites for the recombination of the photogenerated electrons. According to electron spin resonance (ESR) spectroscopic study, the photoexcited electron trap at surface $Ti^{3+}$ sites or $Ti^{4+}$ sites within the bulk and holes trap at lattice oxygen ions [22–24]. Therefore, the bulk defect should be reduced to obtain high photocatalytic activity. The nature of defects on $TiO_2$ can be found in a recent review by Watson et al. [25].

In this study, nano-$TiO_2$ powders with average crystallite sizes in the range of 9–15 nm were synthesized by the solvothermal method. The effect of crystallite size on the

*Corresponding author. Tel.: +66 2218 6882; fax: +66 2218 6877.
*E-mail address:* piyasan.p@chula.ac.th (P. Praserthdam).

0022-0248/$ - see front matter © 2006 Elsevier B.V. All rights reserved.
doi:10.1016/j.jcrysgro.2006.09.018

amount of surface defects on $TiO_2$ was investigated by means of X-ray diffraction (XRD), $N_2$ physisorption, temperature-programmed desorption of $CO_2$, and ESR spectroscopy. Photocatalytic activities of the $TiO_2$ powders were determined from a gas-phase decomposition of ethylene under UV irradiation.

## 2. Experimental Procedure

### 2.1. Preparation of $TiO_2$

Nanocrystalline $TiO_2$ was prepared using the solvothermal method according to that of Ref. [26] using titanium (IV) *n*-butoxide (TNB) as starting material. In general, 15–25 g of TNB was suspended in 100 $cm^3$ of toluene in a test tube, which was then placed in a 300 $cm^3$ autoclave. The gap between the test tube and the autoclave wall was filled with 30 $cm^3$ of the same solvent used in the test tube. The autoclave was purged completely by nitrogen before heating up to 573 K at a rate of 2.5 K/min. Autogeneous pressure during the reaction gradually increased as the temperature was raised. Once the prescribed temperature was reached, the temperature was held constant for 0.5–8 h. After the system was cooled down, the resulting powders were repeatedly washed with methanol and dried in air. The synthesis product was then calcined in a box furnace by heating up to the desired temperature, in the range of 563–583 K, at a rate of 10 K/min and held at that temperature for 1 h in order to remove any impurity that might remain on the samples after washing with methanol.

### 2.2. Characterization

Powder XRD analysis was carried out using a SIEMENS D5000 diffractometer with Cu $K_\alpha$ radiation. The crystallite size of the product was determined from broadening of its main peak ($2\theta = 25°$) using the Scherrer equation. The specific surface area was calculated using Brunauer-Emmett-Teller (BET) single-point method on the basis of nitrogen uptake measured at 77 K at a relative pressure of 0.3. Before $N_2$ adsorption, each sample was dried at 403 K for 30 min in a 30% $N_2$–helium flow. The amount of nitrogen desorbed was measured using a thermal conductivity detector. Temperature-programmed desorption using $CO_2$ as a probe molecule ($CO_2$-TPD) was performed to determine the $Ti^{3+}$ site existing on the surface of a $TiO_2$ particle [27]. The $CO_2$-TPD was carried out using homemade equipment composed of a quartz tube in a temperature-controlled bath connecting to a gas chromatograph (GOW-MAC) with a thermal conductivity detector. Approximately 0.05 g of a $TiO_2$ sample was dosed by 1 vol% $CO_2$ in helium for 1 h and then desorbed from 143 to 273 K with a rate of 21.5 K/min. ESR spectroscopy was conducted using a JEOL JESRE2X ESR spectrometer. The intensity of ESR was calculated using a computer software program ES-PRIT ESR DATA SYSTEM (version 1.6). Transmission electron micrographs of the $TiO_2$ samples were obtained using a JEOL JEM 1220 electron microscope operated at 80 kVa.

### 2.3. Evaluation of photocatalytic activity

The decomposition of ethylene via photocatalytic reaction was employed to evaluate photocatalytic activity of the $TiO_2$ products obtained. Approximately 0.4 g of the synthesized $TiO_2$ was spread in a horizontal quartz reactor. The air containing 0.1% ethylene was continuously supplied at a constant flow rate with a gas hourly space velocity of 120 $h^{-1}$. The reaction temperature was set at 313 K. For each run, an air stream with 0.1% ethylene was first passed through the reactor without illumination until reaching gas–solid adsorption equilibrium (typically 120–180 min) as indicated by identical inlet/outlet ethylene concentration. Then, UV light was illuminated on the surface of the catalyst by using 500 W mercury lamps. The outlet gas was sampled and analyzed at regular intervals by using a SHIMADZU GC-14B gas chromatograph equipped with the flame-ionized detector.

## 3. Results and discussion

In this study, the crystallite size of the solvothermal-derived $TiO_2$ was varied in the range of 9–15 nm by changing the concentrations of TNB, the reaction temperatures, and the holding times. Increasing reaction temperature and holding time resulted in an increase in the average crystallite size of $TiO_2$. The average crystallite sizes and BET surface areas of the obtained $TiO_2$ from various synthesis conditions are given in Table 1. The XRD patterns of all the obtained $TiO_2$ powders are shown in Fig. 1. The characteristic peaks of pure anatase-phase titania were observed at 25, 38, and 48° $2\theta$ [28] without contamination of other phases such as rutile and brookite. The average crystallite sizes of $TiO_2$ were calculated from the full-width at half-maximum of the XRD peak at $2\theta = 25°$ using the Scherrer equation. As the average $TiO_2$ crystallite size increased from 9 to 15 nm, the BET surface areas decreased monotonically from 126 to 51 $m^2/g$. The specific surface areas of the $TiO_2$ samples were also calculated based on the correlation between surface area and crystallite size as follows:

$$S_2 = 6/d\rho,$$

where $d$ is the average crystallite size and $\rho$ is the density of $TiO_2$ (3.84 g $cm^3$) [29].

It is noticed that $S_1$ determined from $N_2$ physisorption was smaller than $S_2$ calculated based on the crystallite size for all the $TiO_2$ samples. This was probably the result of an amorphous-like phase contaminated in the $TiO_2$ particles [11]. Transmission electron microscope (TEM) imaging has been carried out in order to determine the shape of the particles and the existence of amorphous phase. A typical TEM micrograph of the $TiO_2$-9 nm sample is shown in Fig. 2. The TEM images show that the $TiO_2$ products

Table 1
Specific surface areas and average crystallite sizes of the $TiO_2$ samples obtained from various synthesis conditions

| Sample | Amount of TNB in solvent (g) | Temperature (°C) | Holding time (h) | Crystallite size (nm) | Specific surface area ($m^2$/g) | | $S_1/S_2$ |
|---|---|---|---|---|---|---|---|
| | | | | | $S_1$[a] | $S_2$[b] | |
| 1 | 15 | 300 | 0.5 | 9.0 | 126.4 | 170.9 | 0.74 |
| 2 | 25 | 300 | 2.0 | 11.0 | 92.3 | 139.9 | 0.66 |
| 3 | 25 | 320 | 6.0 | 12.5 | 78.2 | 123.1 | 0.64 |
| 4 | 25 | 350 | 6.0 | 14.5 | 53.1 | 106.1 | 0.50 |
| 5 | 25 | 350 | 8.0 | 15.0 | 51.1 | 102.6 | 0.50 |

[a] $S_1$ is specific surface area determined from $N_2$ physisorption results.
[b] $S_2$ is specific surface area calculated based on the correlation between surface area and crystallite size of $TiO_2$ ($S_2 = 6/d\rho$ [29]).

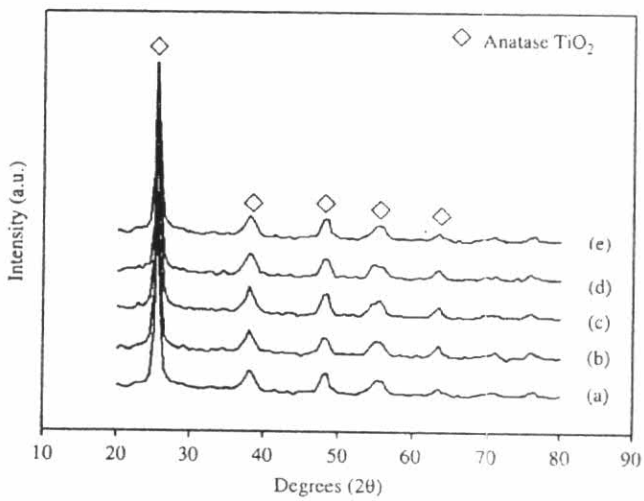


Fig. 1. XRD patterns of the $TiO_2$ samples with various crystallite sizes (a) 9 nm, (b) 11 nm, (c) 12.5 nm, (d) 14.5 nm, and (e) 15 nm.

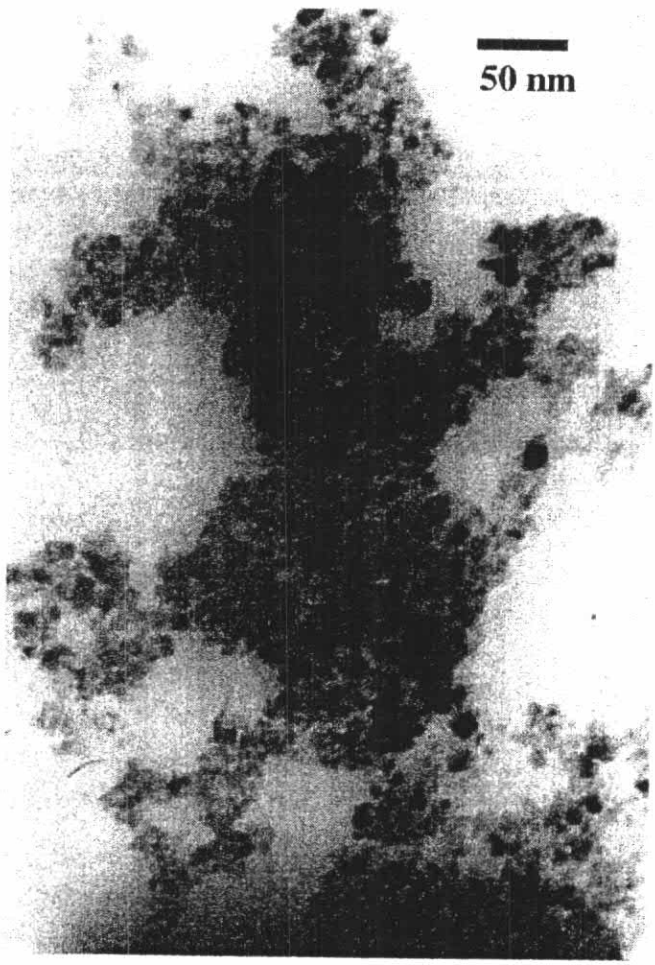


Fig. 2. A typical TEM micrograph of the $TiO_2$-9 nm sample.

obtained by solvothermal synthesis under the conditions used consist of spherical particles with particle sizes consistent with the calculated results. The $TiO_2$ samples may contain a fraction of amorphous phase since the preferential orientation of $TiO_2$ nanoparticles was not clearly seen; however, it is probably due to the moderate magnification used. In order to elucidate the structure of $TiO_2$ nanocrystallites, a high-resolution transmission electron microscope with selected area electron diffraction (SAED) may be needed.

Temperature-programmed desorption profiles of $CO_2$ from the titania surface are shown in Fig. 3. The titania samples exhibited two desorption peaks at temperatures ca. 183 K and 213 K, which were attributed to the two structures of $TiO_2$ [30]. The peak at ca. 183 K is attributed to $CO_2$ molecules bounding to regular five-coordinate $Ti^{4+}$ site, which was considered as the perfect titania structure. The second peak at ca. 213 K has been considered as desorption of $CO_2$ molecules bounding to $Ti^{3+}$ defect structure. It is clearly seen from the TPD results that the areas of the $CO_2$ desorption peak at 213 K apparently increased with increasing crystallite size. It is indicated that the larger crystallite size of $TiO_2$ obtained from solvothermal synthesis possessed a higher amount of $Ti^{3+}$ surface defects. The ratios of peak areas of $Ti^{3+}/Ti^{4+}$ were also determined by curve fitting and area calculation using a SYSTAT Peakfit program and the results are given in Table 2. It was found that the $Ti^{3+}$ density increased with increasing $TiO_2$ crystallite size from 9 to 14.5 nm. The value of $Ti^{3+}/Ti^{4+}$ for $TiO_2$-14.5 nm and $TiO_2$-15 nm was not significantly different.

An example of the ESR results of the solvothermal-derived $TiO_2$ powders is shown in Fig. 4. All the titania samples exhibited one major signal at a $g$ value of 1.996,

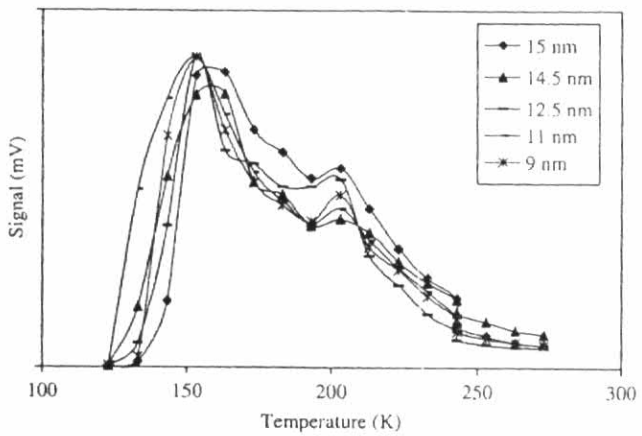


Fig. 3. Thermal desorption spectra for $CO_2$ adsorbed on the various $TiO_2$ samples.

Table 2
Ratios of peak areas of $Ti^{3+}/Ti^{4+}$ determined from the $CO_2$-TPD experiments

| Average crystallite size[a] (nm) | $Ti^{3+}/Ti^{4+}$[b] |
|---|---|
| 9.0 | 0.923 |
| 11.0 | 1.046 |
| 12.5 | 1.299 |
| 14.5 | 1.580 |
| 15.0 | 1.474 |

[a]Based on XRD results.
[b]Based on $CO_2$-TPD results.

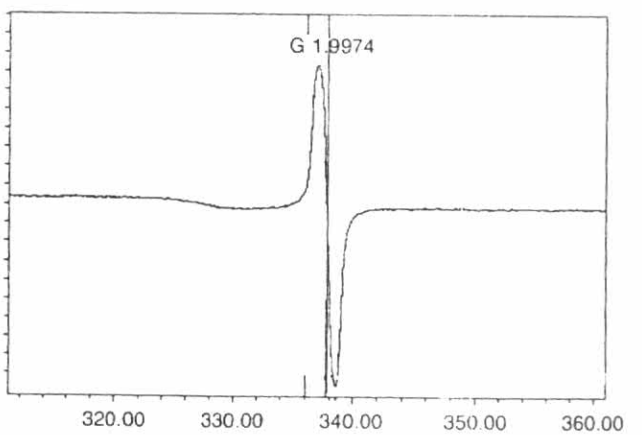


Fig. 4. ESR spectra for various $TiO_2$ samples.

which can be assigned to $Ti^{3+}$ at titania surface [31–33]. According to Nakaoka and Nosaka [24], there were six ESR signals that occurred on the surface of titania: (i) $Ti^{4+}O^{-}Ti^{4+}OH^{-}$, (ii) surface $Ti^{3+}$, (iii) adsorbed oxygen ($O^{2-}$), (iv) $Ti^{4+}O^{2-}Ti^{4+}O^{2-}$, (v) inner $Ti^{3+}$, and (vi) adsorbed water. Fig. 5 demonstrates a relationship between the intensity of ESR spectra per surface area of the $TiO_2$ and the $TiO_2$ average crystallite size. It was found that the amount of surface defect of $TiO_2$ increased with increasing crystallite size.

Photocatalytic decomposition of ethylene was conducted to assess the photocatalytic activity of $TiO_2$ samples with various crystallite sizes. The conversion of ethylene as a function of time-on-stream for all the samples is shown in Fig. 6. In this study, 'time-on-stream' is defined as the time that surface of the catalyst was illuminated by UV light using 500 W mercury lamps. Photocatalytic activities of the various $TiO_2$ crystallite sizes are evidently different; ethylene conversions increased with increasing $TiO_2$ crystallite sizes. It can be correlated to the different amounts of $Ti^{3+}$ defects on $TiO_2$ samples, in which the higher the amount of $Ti^{3+}$ present in $TiO_2$, the higher photocatalytic activity obtained. In photocatalysis, light irradiation of $TiO_2$ powder with photon energy larger than the band-gap energy produces electrons ($e^-$) and holes ($h^+$) in the conduction band and the valence band, respectively. These electrons and holes are thought to have the respective abilities to reduce and oxidize chemical species adsorbed on the surface of $TiO_2$ particles. For a photocatalyst to be most efficient, different interfacial electron processes involving $e^-$ and $h^+$ must compete effectively

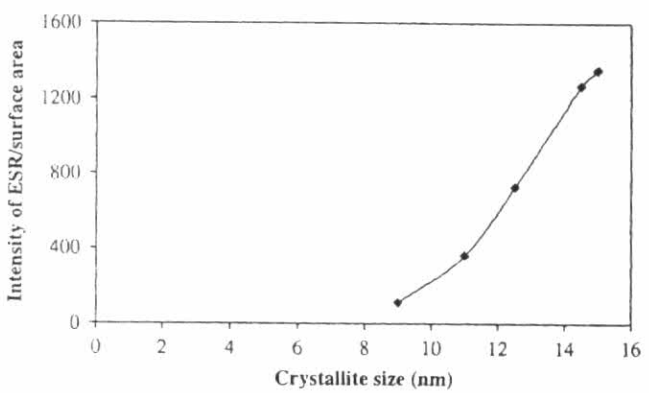


Fig. 5. The intensity of ESR spectra/surface area as a function of $TiO_2$ crystallite size.

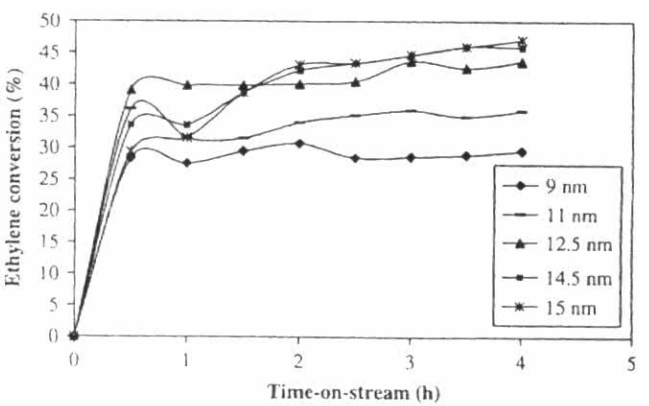


Fig. 6. Photocatalytic activity of the various $TiO_2$.

with the major deactivation processes involving $e^- - h^+$ recombination. In general, $TiO_2$ with higher crystallinity and higher specific surface area typically shows higher photocatalytic activity since the defect of crystal can be the recombination center of the electron–hole pair; hence the photocatalytic activity decreases [1,34,35]. However, the role of $Ti^{3+}$ surface defects on photocatalytic activity of $TiO_2$ is different from that of crystal (bulk) defect. The $Ti^{3+}$ surface defects serve as traps for photogenerated electrons and consequently prolong lifetime of holes, resulting in higher photocatalytic activity [36–38].

## 4. Conclusions

This work showed the impact of crystallite size of $TiO_2$ in the range of 9–15 nm on the $Ti^{3+}$ surface defect present in $TiO_2$ powders. The amounts of $Ti^{3+}$ defects as determined by ESR and $CO_2$-TPD were found to increase with increasing crystallite size of $TiO_2$. The photocatalytic activity of $TiO_2$ also increased in a similar trend due to an increase in the surface defect/specific surface area of the $TiO_2$ samples.

## Acknowledgments

The authors would like to thank the Thailand Research Fund (TRF), the Commission on Higher Education, and the TJTTP-JBJC for the financial supports of this project.

## References

[1] B. Ohtani, Y. Ogawa, S. Nishimoto, J. Phys. Chem. B 101 (1998) 3746.
[2] J.-M. Herrmann, C. Guillard, J. Disdier, C. Lehaut, S. Malato, J. Blanco, Appl. Catal. B-Environ. 35 (2002) 81.
[3] M. Bekbolet, A.S. Suphandag, C.S. Uyguner, J. Photochem. Photobiol. A: Chem. 148 (2002) 121.
[4] J. Aguado, R. Van Grieken, M.J. López-Muñoz, J. Marugán, Catal. Today 75 (2002) 95.
[5] G. Sivalingam, K. Nagaveni, M.S. Hegde, G. Madras, Appl. Catal. B-Environ. 45 (2003) 23.
[6] V.A. Sakkas, I.M. Arabatzis, I.K. Konstantinou, A.D. Dimou, T.A. Albanis, P. Falaras, Appl. Catal. B-Environ. 49 (2004) 195.
[7] D.P. Das, K. Parida, B.R. De, J. Mol. Catal. A-Chem. 240 (2005) 1.
[8] C.-S. Kim, B.K. Moon, J.-H. Park, S.T. Chung, S.-M. Son, J. Crystal Growth 254 (2003) 405.
[9] C. Wang, Z.-X. Deng, G. Zhang, S. Fan, Y. Li, Powder Technol. 125 (2002) 39.
[10] M. Kang, B.-J. Kim, S.M. Cho, C.-H. Chung, B.-W. Kim, G.Y. Han, K.J. Yoon, J. Mol. Catal. A-Chem. 180 (2002) 125.
[11] H. Kominami, M. Kohno, Y. Takada, M. Inoue, T. Inui, Y. Kera, Ind. Eng. Chem. Res. 38 (1999) 3925.
[12] H.-D. Nam, B.-H. Lee, S.-J. Kim, C.-H. Jung, J.-H. Lee, S. Park, Jpn. J. Appl. Phys. 37 (1998) 4603.
[13] C. Su, B.-Y. Hong, C.-M. Tseng, Catal. Today 96 (2004) 119.
[14] P. Yang, C. Lu, N. Hua, Y. Du, Mater. Lett. 57 (2002) 794.
[15] Y. Bessekhouad, D. Robert, J.V. Weber, J. Photochem. Photobiol. A: Chem. 157 (2003) 47.
[16] H. Kominami, J.-I. Kalo, Y. Takada, Y. Doushi, B. Ohtani, S.-I. Nishimoto, M. Inoue, Y. Kera, Catal. Lett. 46 (1997) 235.
[17] O. Carp, C.L. Huisman, A. Reller, Prog. Solid State Chem. 32 (2004) 33.
[18] T. Torimoto, R.J. Fox III, M.A. Fox, J. Electrochem. Soc. 143 (1996) 3712.
[19] V. Shklover, M.-K. Nazeeruddin, S.M. Zakeeruddin, C. Barbé, A. Kay, T. Haibach, W. Steurer, M. Grätzel, Chem. Mater. 9 (1997) 430.
[20] A.-K. Axelsson, L.J. Dunne, J. Photochem. Photobiol. A: Chem. 144 (2001) 205.
[21] G. Liu, J.A. Rodriguez, J. Hrbek, B.T. Long, D.A. Chen, J. Mol. Catal. A-Chem. 202 (2003) 215.
[22] R.F. Howe, M. Gratzel, J. Phys. Chem. 89 (1985) 4495.
[23] R.F. Howe, M. Gratzel, J. Phys. Chem. 91 (1987) 3906.
[24] Y. Nakaoka, Y. Nosaka, J. Photochem. Photobiol. A: Chem. 110 (1997) 299.
[25] U. Diebold, J. Lehman, T. Mahmoud, M. Kuhn, G. Leonardelli, W. Hebenstreit, M. Schmid, P. Varga, Surf. Sci. 411 (1998) 137.
[26] M. Inoue, H. Kominami, T. Inui, J. Chem. Soc. Dalton Trans. (1991) 3331.
[27] T.L. Thompson, O. Diwald, J.T. Yates Jr., J. Phys. Chem. B 107 (2003) 11700.
[28] S.S. Watson, D. Beydoun, J.A. Scott, R. Amal, Chem. Eng. J. 95 (2003) 213.
[29] W. Payakgul, O. Mekasuwandumrong, V. Pavarajarn, P. Praserthdam, Ceram. Inter. 31 (2005) 391.
[30] L.T. Tracy, D. Oliver, T.Y. John, J. Phys. Chem. B 107 (2003) 11700.
[31] K.-R. Park, J. Zhang, K. Ikeue, H. Yamashita, M. Anpo, J. Cataly. 185 (1999) 114.
[32] A. Watterich, A. Hofstaetter, R. Wuerz, A. Scharmann, J. Solid State Commun. 100 (1996) 513.
[33] Y. Zeng, Y. Zheng, S. Yu, K. Chen, S. Zhou, J. Electrochem. Comm. 4 (2002) 293.
[34] K.Y. Jung, S.B. Park, J. Photochem. Photobiol. A: Chem. 127 (1999) 117.
[35] M.I. Litter, Appl. Catal. B-Environ. 23 (1999) 89.
[36] G. Lu, A. Linsebigler, J.T. Yates Jr., J. Phys. Chem. 99 (1995) 7626.
[37] J. Schwitzgebel, J.G. Ekerdt, H. Gerischer, A. Heller, J. Phys. Chem. 95 (1995) 5633.
[38] D. Brinkley, T. Engel, Surf. Sci. 415 (1998) 1001.

Jointly published by
Akadémiai Kiadó, Budapest
and Springer, Dordrecht

React Kinet Catal Lett
Vol. 91, No. 1, 119–126 (2007)
10.1007/s11144-007-5076-6

RKCL5076

# EFFECT OF $TiO_2$ CRYSTALLITE SIZE ON THE DISPERSION OF Co ON NANOCRYSTALLINE $TiO_2$

**Wilasinee Kongsuebchart, Joongjai Panpranot, Chairit Satayaprasert and Piyasan Praserthdam***
Center of Excellence on Catalysis and Catalytic Reaction Engineering,
Department of Chemical Engineering, Chulalongkorn University, Bankok 10330 Thailand

*Received January 2, 2007, accepted January 16, 2007*

**Abstract**

Nanocrystalline $TiO_2$ powders with average crystallite sizes of 9-15 nm were synthesized by the solvothermal method and employed as supports for Co catalysts. The value of $H_2$ chemisorption/specific surface area of $Co/TiO_2$ increased significantly with increasing $TiO_2$ crystallite size. It was suggested that the higher amount of $Ti^{3+}$ surface defects on the larger crystalline $TiO_2$ resulted in a stronger interaction between Co and $TiO_2$, hence, higher dispersion of Co was obtained.

*Keywords*: $TiO_2$, solvothermal, crystallite size, cobalt catalyst, dispersion

## INTRODUCTION

Titanium dioxide ($TiO_2$) is a very useful material and has received great attention in catalysis research as catalyst, catalyst support, and promoter. It is one of

* Corresponding author. Tel: 662-2186883; Fax: 662-2186877; E-mail: piyasan.p@chula.ac.th
0133-1736/2007/US$ 20.00.

the most promising catalysts in photocatalytic applications [1-3]. In addition, as a catalyst support particularly in hydrogenation reactions, $TiO_2$ manifests a strong metal-support interaction (SMSI) with group VIII metals resulting in an improved catalytic performance [4-5]. It has been reported that $Co/TiO_2$ shows high activities in CO hydrogenation and gives a distribution of Fischer-Tropsch products ranging from $C_1$ to $C_{18+}$ hydrocarbons with high selectivity for $C_2$-$C_{11}$ [6].

However, the physical and chemical properties of $TiO_2$ can be modified when they are synthesized in the nanometer range [7]. Nanocrystalline $TiO_2$ with high specific surface area is thus desirable for the preparation of $TiO_2$ supported catalysts with high metal dispersion.

In this study, nanocrystalline $TiO_2$ with various crystallite sizes in the range of 9-15 nm were synthesized by the solvothermal method. This technique allows a one-step synthesis of pure nano-sized anatase $TiO_2$. The effect of $TiO_2$ crystallite size on the dispersion of cobalt on $TiO_2$ was investigated by various analytical techniques such as X-ray diffraction, electron spin resonance spectroscopy, $N_2$ physisorption, and $H_2$ chemisorption.

## EXPERIMENTAL

### Preparation of $TiO_2$ and $Co/TiO_2$ catalysts

Nanocrystalline $TiO_2$ was prepared by using the solvothermal method according to Ref. [8] using titanium(IV) *n*-butoxide (TNB) as starting material. In general, an amount of 15-25 g of TNB was suspended in 100 $cm^3$ of toluene in a test tube, which was then placed in a 300 $cm^3$ autoclave. The gap between the test tube and the autoclave wall was filled with 30 $cm^3$ of the same solvent used in the test tube. The autoclave was purged completely by nitrogen before heating up to the desired temperature, in the range of 573-623 K, at a rate of 10 K/min. Once the prescribed temperature was reached, the temperature was kept constant for 0.5-8 h. After the system was cooled down, the resulting powders were repeatedly washed with methanol and dried in air. The synthesis product was then calcined in a box furnace by heating up to the desired temperature, in the range of 563-583 K, at a rate of 10 K/min and kept at that temperature for 1 h. $Co/TiO_2$ catalysts with approximately 20 wt.% Co were prepared by incipient wetness impregnation using $Co(NO_3)\cdot 6H_2O$ (Aldrich) as cobalt precursor. The catalysts were dried at 383 K for 12 h and calcined in air at 723 K for 4 h prior to use.

### Characterization

The specific surface area of the samples was calculated using the Brunauer-Emmett-Teller (BET) single point method. Approximately 0.3-0.5 g of the catalyst sample was placed in the sample cell and heated up to 473 K and kept at that temperature for 10 h under 30% $N_2$ in He flow. The catalyst sample was then cooled down to room temperature and was dipped into liquid nitrogen. After equilibrium adsorption of nitrogen, the sample cell was dipped into a water bath at room temperature. The amount of nitrogen desorbed was measured by a gas chromatograph (GOW-MAC). X-ray diffraction was carried out by using a SIEMENS D5000 X-ray diffractometer, using Cu $K_\alpha$ radiation with a Ni filter in the 20-80°2θ angular regions. Electron spin resonance spectroscopy (ESR) was conducted using a JEOL JESRE2X electron spin resonance spectrometer. The intensity of ESR was calculated using a computer software program ES-PRIT ESR DATA SYSTEM (version 1.6). $H_2$-chemisorption was carried out by using a Micromeritics Pulse Chemisorb 2700 instrument at 373 K on the reduced catalysts. Prior to chemisorption, the catalysts were reduced at 623 K for 10 h.

## RESULTS AND DISCUSSION

The properties of various nanocrystalline $TiO_2$ prepared via solvothermal synthesis are shown in Table 1. The average crystallite size of $TiO_2$ can be tailored by changing the concentration of titanium *n*-butoxide, reaction temperature, and time. Typically, increasing the titanium butoxide concentration, reaction temperature, and/or reaction time resulted in an increase in the average crystallite size of $TiO_2$. From the XRD results (Fig. 1), only pure anatase phase $TiO_2$ was observed for all the samples at 2θ of 25, 38, and 48° [9]. The average crystallite sizes of $TiO_2$ were calculated from the full width at half maximum of the XRD main peak at $2\theta = 25°$ using the Scherrer equation. While the average $TiO_2$ crystallite size increased from 9 to 15 nm, the BET surface areas decreased monotonically from 126 to 51 $m^2/g$. Electron spin resonance spectroscopy was conducted in order to monitor the $Ti^{3+}$ defects on the $TiO_2$ surface. A typical ESR spectrum of the nanocrystalline $TiO_2$ prepared by the solvothermal method is shown in Fig. 2. All the nanocrystalline $TiO_2$ samples exhibited only one main signal at a *g* value of 1.996 which can be assigned to $Ti^{3+}$ defective sites of $TiO_2$ at the surface [10-12]. Nakaoka *et al.* [13] has reported six signals in the ESR measurement occurring on the surface of titania: (i) $Ti^{4+}O^-Ti^{4+}OH^-$, (ii) surface $Ti^{3+}$, (iii) adsorbed oxygen ($O^{2-}$), (iv) $Ti^{4+}O^{2-}$ $Ti^{4+}O^{2-}$, (v) inner $Ti^{3+}$, and (vi) adsorbed water. The relationship of ESR intensity/BET surface area of the $TiO_2$ as a function of $TiO_2$ crystallite size is

illustrated in Fig. 3. It was found that for a given surface area, the amount of surface defects on $TiO_2$ significantly increased with increasing crystallite size.

**Table 1**

Properties of various nanocrystalline $TiO_2$ samples synthesized by the solvothermal method

| | Preparation conditions | | | Average crystallite size | Specific surface area |
|---|---|---|---|---|---|
| | TNB amount (g) | Temp. (°C) | Reaction time (h) | (nm) | ($m^2/g$) |
| 1 | 15 | 300 | 0.5 | 9.0 | 126 |
| 2 | 25 | 300 | 2 | 11.0 | 92 |
| 3 | 25 | 320 | 6 | 12.5 | 78 |
| 4 | 25 | 350 | 6 | 14.5 | 53 |
| 5 | 25 | 350 | 8 | 15.0 | 51 |

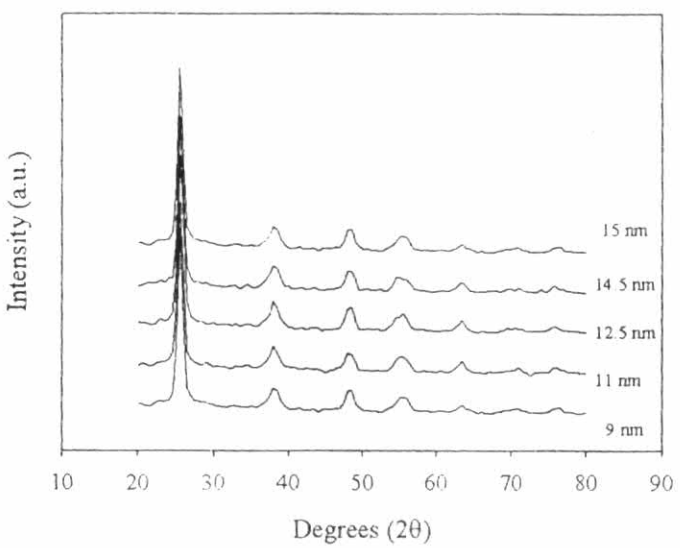


**Fig. 1.** XRD patterns of nanocrystalline $TiO_2$ synthesized by the solvothermal method

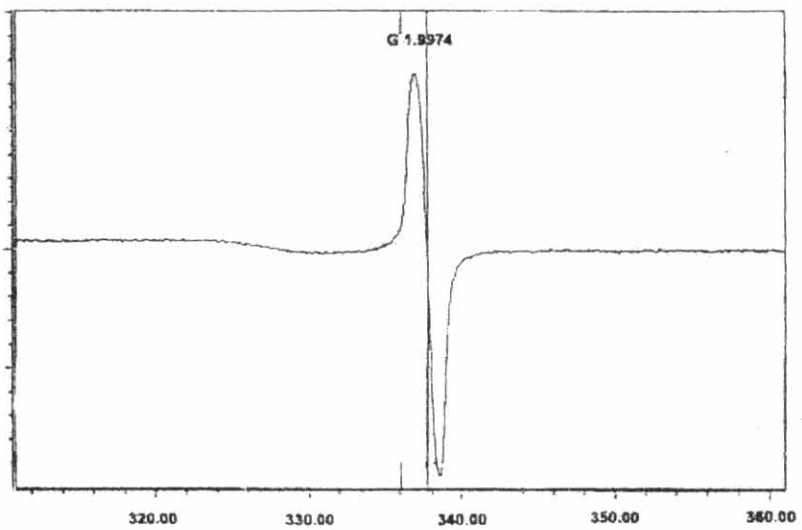


**Fig. 2.** A typical ESR results of the solvothermal-derived $TiO_2$

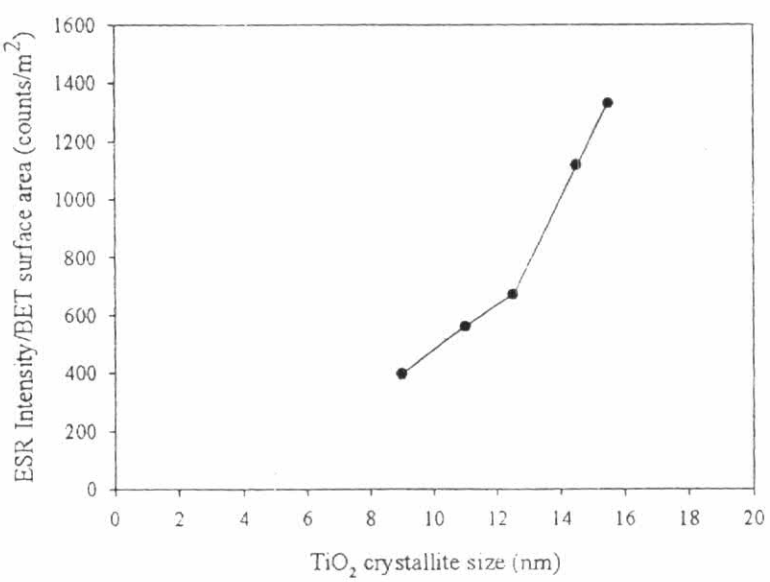


**Fig. 3.** ESR intensity/BET surface area as a function of $TiO_2$ crystallite size

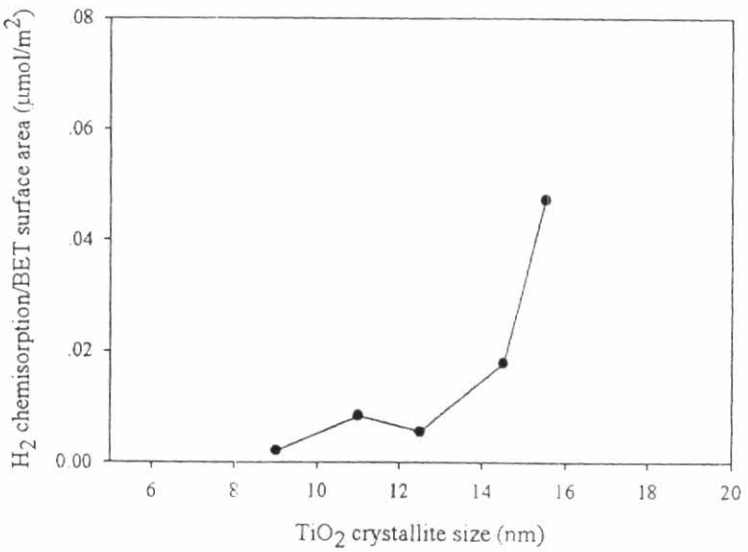


**Fig. 4.** $H_2$ chemisorption/BET surface area as a function of $TiO_2$ crystallite size

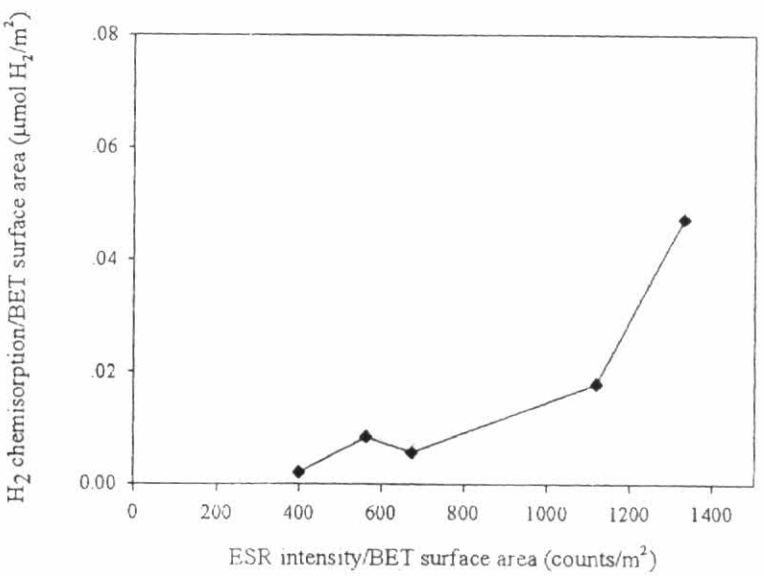


**Fig. 5.** Relationship between ESR intensity/BET surface area and $H_2$ chemisorption/BET surface area of the $Co/TiO_2$ catalysts

It is known that only surface cobalt metal atoms are active for CO hydrogenation reaction and not its oxide or carbide [14]. The relative amounts of active cobalt metal atoms on the $Co/TiO_2$ catalyst samples were calculated from $H_2$ chemisorption experiments at 100°C according to Bartholomew *et al.* [15]. In general, the catalyst with a higher BET surface area exhibits $H_2$ chemisorption and Co dispersion. Thus, in order to separate the effect of BET surface area on Co dispersion from the effect of $TiO_2$ crystallite size, the amounts of $H_2$ chemisorption are reported in terms of micromole $H_2$ chemisorption per unit surface area. Such relationship is shown in Fig. 4. It was found that for a given surface area, the amount of $H_2$ chemisorption on the $Co/TiO_2$ catalysts significantly increased with increasing crystallite size, especially when the $TiO_2$ crystallite sizes were in the range of 14.5-15 nm. Figure 5 shows the relationship between ESR intensity/BET surface area and $H_2$ chemisorption/BET surface area. A similar trend was observed; as the ESR intensity/BET surface area increased, the $H_2$ chemisorption/BET surface area also increased. Such results suggest that increasing the amount of surface $Ti^{3+}$ defects of $TiO_2$ can result in higher amount of active Co dispersed on the solvothermal-derived nanocrystalline $TiO_2$.

It has been reported that the binding energy for metal and $TiO_2$ is larger at the oxygen defect sites than at the normal sites of the $TiO_2$ surface [16]. Therefore, the solvothermal-derived $TiO_2$ with larger crystallite sizes (higher amounts of $Ti^{3+}$ surface defects) can result in stronger interaction of the $TiO_2$ surface and the cobalt precursor, and consequently, higher dispersion of Co on the $TiO_2$ supports. For the synthesis of highly dispersed cobalt catalysts on alumina, Zhang *et al.* [17] suggested that a strong interaction was required between the support and cobalt precursor. In a recent study from our group [18], the $TiO_2$ surface when modified by different pre-treatments resulted in $TiO_2$ samples with different amounts of $Ti^{3+}$ defects on the surface. The Co catalysts supported on the $TiO_2$ containing higher amount of $Ti^{3+}$ also exhibited higher Co dispersion. The results in this study, thus, confirm the effect of $Ti^{3+}$ defective sites present on the nanocrystalline $TiO_2$ surface, which as itself is a function of the $TiO_2$ crystallite size, thus also on the dispersion of active Co metal on $TiO_2$ surfaces.

**Acknowledgements.** Financial support from the Commission on Higher Education is gratefully acknowledged.

## REFERENCES


1. B. Ohtani, Y. Ogawa, S.J. Nishimoto: *J. Phys. Chem. B*, **101**, 3746 (1997).
2. U. Stafford, K. A. Gray, P.V. Kamat: *J. Catal.*, **167**, 25 (1997).
3. J.-M. Herrmann: *Catal. Today*, **53**, 115 (1999).
4. S.J. Tauster, S.C. Fung, R.L. Garten: *J. Am. Chem. Soc.*, **100**, 170 (1978).
5. J.H. Kang, E.W. Shin, W.J. Kim, J.D. Park, S.H. Moon: *J. Catal.*, **208**, 310 (2002).
6. N.J. Coville, J. Li: *Catal. Today*, **71**, 403, (2002).
7. U. Diebold: *Surf. Sci. Rep.*, **48**, 53 (2003).
8. M. Inoue, H. Kominami, T. Inui: *J. Chem. Soc. Dalton Trans.*, 3331–3336 (1991).
9. S.S. Watson, D. Beydoun, J.A. Scott, R. Amal: *Chem. Eng. J.*, **95**, 213 (2003).
10. K.-R. Park, J. Zhang, K Ikeue, H. Yamashita, M. Anpo: *J. Catal.*, **185**, 114 (1999).
11. A. Watterich, A. Hofstaetter, R. Wuerz, A. Scharmann: *J. Solid State Commun.*, **100**, 513 (1996).
12. Y. Zeng, Y. Zheng, S. Yu, K. Chen, S. Zhou: *J. Electrochem. Commun.*, **4**, 293 (2002).
13. T.L. Thompson, O. Diwald, J.T. Yates: *J. Phys. Chem. B*, **107**, 11700 (2003).
14. R.B. Anderson: *The Fischer-Tropsch Synthesis*, Academic Press, San Diego, (1984).
15. R.C. Reuel, C.H. Bartholomew: *J. Catal.*, **85**, 78 (1984).
16. W. Nae-Lih, L. Min-Shuei, P. Zern-Jin, H. Jin-Zern: *J. Photochem. Photobiol. A*, **163**, 277 2004.
17. Y. Zhang, D. Wei, S. Hammache, J.G. Goodwin, Jr.: *J. Catal.*, **188**, 281 (1999).
18. K. Suriye, P. Praserthdam, B. Jongsomjit: *Ind. Eng. Chem. Res.*, **44**, 6599 (2005).

# VITAE

Miss Wilasinee Kongsuebchart was born on November 26th, 1975 in Nakhon Ratchasima, Thailand. She received the Bachelor degree of Engineering with a major in Chemical Engineering from Khonkaen University in May 1997 and her Master degree at the department of Chemical Engineering, Khonkaen University in May 2001. She was continuous to study at Chulalongkorn University in October 2003.